AMERICAN UNIVERSITY OF BEIRUT

EFFECT OF THE MAGNETIC FIELD ON THE EARLY COLLAPSE PHASE OF A DENSE PROTOSTELLAR CLOUD

by

CYNTHIA RAYMOND SAAD

A thesis
submitted in partial fulfillment of the requirements
for the degree of Master of Science
to the Department of Physics
of the Faculty of Arts and Sciences
at the American University of Beirut

Beirut, Lebanon
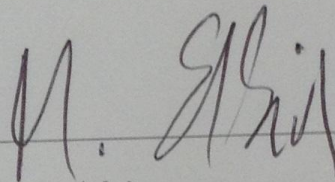December 2015

AMERICAN UNIVERSITY OF BEIRUT

EFFECT OF THE MAGNETIC FIELD ON THE EARLY COLLAPSE PHASE OF A DENSE PROTOSTELLAR CLOUD

by
CYNTHIA RAYMOND SAAD

Approved by:
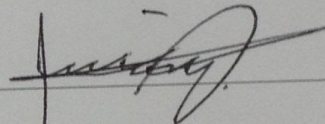
_____

Dr. Mounib El Eid, Professor   Advisor

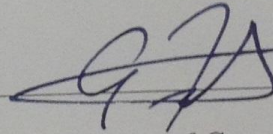Physics

_____

Dr. Jihad Touma, Professor   Member of Committee

Physics

_____

Dr. Ghassan Antar, Associate Professor   Member of Committee

Physics

Date of thesis defense: December 8, 2015

AMERICAN UNIVERSITY OF BEIRUT

THESIS RELEASE FORM

Student Name: ___Saad_____Cynthia_____Raymond_____
                            Last   First   Middle

☑ Master's Thesis   ◯ Master's Project   ◯ Doctoral Dissertation

☑   I authorize the American University of Beirut to: (a) reproduce hard or electronic copies of my thesis, dissertation, or project; (b) include such copies in the archives and digital repositories of the University; and (c) make freely available such copies to third parties for research or educational purposes.

☐   I authorize the American University of Beirut, **three years after the date of submitting my thesis, dissertation, or project,** to: (a) reproduce hard or electronic copies of it; (b) include such copies in the archives and digital repositories of the University; and (c) make freely available such copies to third parties for research or educational purposes.

_____January 12, 2016_____

Signature   Date

ACKNOWLEDGMENTS

world. Their commitment to open science has helped make this work possible.

An Abstract of the Thesis of

Cynthia Raymond Saad   for   <u>Master of Sciences</u>
<u>Major</u>: Physics

Title: <u>Effect of the magnetic field on the early collapse phase of a dense protostellar</u>
<u>cloud</u>

The purpose of this study is to investigate the role of magnetic field on the first collapse of rotating molecular clouds.

The process of ambipolar diffusion has been considered and analyzed. Order of magnitude estimates are presented to justify the use of the ideal MHD approach to study the initial collapse phase in our work.

As a first step, an isothermal magnetized and rotating sphere of uniform density was considered. More realistic initial conditions were used consisting of a centrally condensed cloud with a barotropic equation of state. A small perturbation was introduced to the clouds and a three-dimensional MHD code was used to study the effect of the variable magnetic field strengths suggested by observations.

The results obtained in this work suggest that the magnetic field is a supporting agent against gravitational collapse as expected. Furthermore, the initial strength of the magnetic field determines whether the stellar cloud undergoes fragmentation into multiple objects.

We propose some ideas for future work taking the advantage of multidimensional simulation. In particular, it is interesting to study the process of star formation under the conditions leading to the formation of the first stars in the universe.

Contents

List of Figures

List of Tables

Chapter 1

Introduction

This chapter describes the molecular clouds as the site of star formation. We introduce several physical processes involved in this fundamental process in astrophysics.

1.1 Molecular clouds

Molecular clouds are considered to be the major site of star formation in the interstellar medium. They represent the coldest and densest components in the interstellar medium. They are large associations of molecular hydrogen, Helium and traces of heavier elements. These clouds are characterized by relatively high number densities in the range $(10^3 cm^{-3} - 10^4 cm^{-3})$ and relatively low temperatures about 10 K. Cores inside them could have even higher densities between $(10^5 cm^{-3} - 10^6 cm^{-3})$. Their sizes are in the range (1-5) parsec where 1pc is 3.26 lightyears, and masses of the order of 10^4 solar masses (Myers, 1985). The aver-

age time required to collect gas into giant molecular clouds is about 30 Myr in the Galactic average or 50Myr in the solar neighborhood. Whereas, the cloud's lifetime is about 20Myr (Larson, 1993).

The molecular clouds are subject to energetic cosmic rays of energies $> 100MeV$ leading to the ionization of neutral particles. However, cosmic rays are able to ionize a small fraction of neutral particles, about 10^{-7} particle/s.

Due to their low temperature, molecular clouds are also called dark clouds. Since molecular hydrogen does not have a permanent magnetic dipole moment (it is called homo-nuclear), the first allowed transition is from the rotationally excited state of J=2 to the ground state. However, at such low temperatures, the occupation of J=2 is extremely small of the order of 10^{-22}. Therefore, molecular clouds with these properties are called dark cloud (Krumholz, 2011). This is in contrast with the atomic hydrogen, for which the hyperfine transition leading to the 21cm wavelength corresponds to an average temperature of 0.068 K and thus can occur even in coldest region of the cloud.

Another property of molecular clouds is that they are magnetized. Their magnetic field strengths is a function of their neutrals number density (see figure (3.1)). For instance, for $n_H = [10^3 - 10^5 cm^{-3}]$, the magnetic field strength ranges between 10 and $100\mu G$ (Crutcher, 2012).

1.2 Star formation time line

The time scale of star formation can be divided into three phases. A first phase is a contraction toward the formation of a protostar. This phase is followed by a second one when a hydrostatic protostar is formed and starts accreting mass. When the mass accretion stops, a contraction third phase starts on a Kelvin-Helmholtz time scale that is a time scale determined by gravitational contraction at constant mass. This phase is associated with the T Tauri stars, which became observable and evolve finally to the zero-age main sequence, where hydrogen burns under hydrostatic and thermal conditions.

One important question is whether the time scale of the formation of the T Tauri star measures the time of the whole formation process?. It seems (Tassis & Mouschovias, 2004) that neglecting the first phase would be a serious underestimation of the time scale of stellar formation. As described in section section:ADtimescale, the ambipolar diffusion would affect the time scale of star formation.

A controversial issue is the duration of the first phase compared to the last T Tauri phase. According to Mouschovias, et al. (2006), the time scale of the first phase can be longer than the last one. So it is not correct to identify the timescale of the star formation with the timescale of the formation of the T Tauri star. Instead it is crucial for the time line to start with a coreless cloud rather than with a hydrostatic protostar.

Chapter 2

Standard theory of star formation

In this chapter, we focus on the first phase of star formation and describe the conditions under which the magnetized molecular cloud collapses to form a protostar.

2.1 Jeans criterion

Star formation is initiated by the gravitational collapse of a large molecular cloud or even a region of the cloud.

The total energy (E_{tot}) of the cloud is the kinetic energy (E_K) and gravitational potential energy (E_{grav}).

If $E_K < |E_{grav}|$, or $E_{tot} < 0$, the cloud is bound and may collapse.

The Jeans criterion (Jeans, 1902) is a simple argument that indicates the collapse

of a gas cloud. The total energy is:

$$E_{tot} = E_K + E_{grav} \tag{2.1}$$

$$E_{tot} < 0 \tag{2.2}$$

$$E_K < -E_{grav} \tag{2.3}$$

Since $E_{grav} < 0$, this equivalent to $E_K < |E_{grav}|$.

This kinetic energy limit requires a relatively cold cloud in order to form stars. The Jeans criterion can be expressed in terms of a limit on the mass and density of the cloud.

Consider a sphere of uniform density, its gravitational potential energy is:

$$E_{grav} = -\frac{3}{5}\frac{GM^2}{R} \tag{2.4}$$

However, the factor 3/5 is in reality larger towards the center , therefore one can use approximately

$$E_{grav} = -\frac{GM^2}{R} \tag{2.5}$$

The kinetic energy of N particles in the cloud is $E_K = \frac{3}{2}NkT$. Then the Jeans criterion reads:

$$\frac{3}{2}NkT < \frac{GM^2}{R} \tag{2.6}$$

Using $M = N\mu m_H$ and $R = \left(\dfrac{3M}{4\pi\rho}\right)^{1/3}$ and some rearrangements, one obtains the relation:

$$M > \left(\frac{3kT}{2\mu m_H G}\right)^{3/2} \left(\frac{3}{4\pi\rho}\right)^{1/2} \equiv M_J \qquad (2.7)$$

M_J is the Jeans mass, which is the minimum value of the cloud mass to undergo gravitational collapse for given composition T and ρ.

It is important to notice that $M_J \propto T^{3/2}\rho^{-1/2}$. The collapse timescale t_{ff} when $M > M_J$ is the time a mass element at the cloud surface needs to reach the centre, which is given by equation (2.18).

Following the collapse, the density has to increase, because the cloud is shrinking, that is the volume decreases but the mass remains unchanged. Concerning the temperature T, the situation is different: its evolution depends on the exchange of energy between the clouds and its surroundings.

The matter in the cloud is heated by cosmic rays penetrating the cloud and ionizing the atoms. Also the liberated electrons due to ionization may collide to the atoms to ionize them as well.

On the other hand, the cloud can be cooled by radiation. Cooling processes seem to be efficient with a consequence that the cloud will be in good approximation isothermal.

A consequence of this is that since T stays constant and ρ increases, the Jeans mass M_J decreases. If there are within the cloud inhomogeneities with mass larger than M_J, they will collapse with there local t_{ff} different from the initial t_{ff} . this process is called "fragmentation" .

2.2   The role of the magnetic field

A magnetic field supports the cloud against gravitational collapse. The question is whether this magnetic support is capable of inhibiting the collapse of the cloud. Also, is it possible for a previously supported cloud to eventually undergo collapse?

Despite the fact that the origin of the magnetic field in the interstellar medium is still not well known, its effect on the process of star formation is worth studying. For a gas cloud with typical temperature T=10K and density $n_H \geq 50cm^{-3}$, the Jeans mass can be estimated to be $M_J \leq 80M_\odot$ and the free fall time (see Eq. 2.18) is $t_{ff} \leq 5 \times 10^6 yrs$. Assuming the thermal pressure is the only support against gravitational collapse, free fall collapse would lead to a galactic star formation rate of $\dot{M}_* \geq 200M_\odot yr^{-1}$, which is far in excess of the observed galactic average of approximately $3M_\odot yr^{-1}$(Braiding, 2011).

Also, observations of individual cores indicate that the non-thermal motions within the cores are subsonic (Benson & Myers, 1989), (Fuller & Myers, 1992), indicating that these motions are unlikely to contribute to the support of the cores against their self-gravity. This is because random supersonic motion is a supporting agent against gravity (Klessen, Heitsch, & Mac Low, 2000).

Hence, in general, molecular clouds must be supported by another mechanism (Zuckerman and Palmer (1974), Ward-Thompson et al. (2007)). Various alternatives to thermal pressure support of molecular clouds have been suggested: magnetic fields (e.g. Chandrasekhar and Fermi (1953), Basu and Mouschovias (1994),

Adams and Shu (2007)), rotation (e.g. Field (1982), N. J. Evans (1999)) and turbulence (e.g. Norman and Silk (1980), Mac Low and Klessen (2004), Vázquez-Semadeni et al. (2007)). These effects may play a role, but the magnetic field is mostly important (Braiding, 2011).

Based on the strength and nature of magnetic field in molecular clouds, there are three theoretical models for star formation:(Crutcher, 2012)

1. **Models with strong field:**

   In this model, the magnetic pressure is sufficiently strong to counteract gravity and prevent gravitational collapse. The ionized gas remains frozen into the field, while the neutral gas and dust contract gravitationally through the field and the ions, increasing the mass in the cloud cores. In this process which is called "ambipolar diffusion", the magnetic field strength than the mass.

2. **Models with weak field:**

   If the magnetic fields are sufficiently weak (then the low-density cloud is super-critical, and the cloud will collapse in roughly the free-fall timescale. Although magnetic pressure cannot stop the collapse, it can dominate turbulent pressure during the late stages of core collapse.

3. **Significant turbulent magnetic field:** Turbulence mainly enhances ambipolar diffusion rate, i.e. allows collapse of a subcritical cloud: the star-formation timescale is reduced by an order of magnitude for a subcritical cloud (Nakamura & Li, 2005).

How does the magnetic field support the cloud against gravitational col-

lapse? It could do so in two ways:

1. The magnetic pressure adds up to the gas pressure to support the cloud against gravitational collapse.

2. The magnetic tension reduces forces due to self-gravity once collapse proceeds and a thin disk forms (Basu, 1997), (Li & Shu, 1997). We can safely ignore this effect in the early collpase phase before the disks form.

The effect of the magnetic field investigated in this work is considered through the magnetic pressure. It is possible to eliminate the magnetic tension contribution if one assumes an initially aligned magnetic field along the $\hat{z}$-axis i.e. $\mathbf{B} = (0, 0, B_z)$. Given this configuration of the magnetic field, the magnetic tension vanishes from the MHD momentum equation (A. P. Boss, 1997). The momentum equation is given by:

$$\rho \frac{\partial \boldsymbol{u}}{\partial t} + \rho \boldsymbol{u}.\boldsymbol{\nabla} \boldsymbol{u} = -\rho \boldsymbol{\nabla} \Phi - \boldsymbol{\nabla} P + \frac{1}{4\pi} \left(\boldsymbol{\nabla} \times \boldsymbol{B} \right) \times \boldsymbol{B} \qquad (2.8)$$

The last term of Eq. 2.8 represents the Lorentz force. To find it, we use the following vector identity:

$$\frac{1}{2} \boldsymbol{\nabla} \left(\boldsymbol{B}.\boldsymbol{B} \right) = \left(\boldsymbol{B}.\boldsymbol{\nabla} \right) \boldsymbol{B} + \boldsymbol{B} \times \left(\boldsymbol{\nabla} \times \boldsymbol{B} \right) \qquad (2.9)$$

This gives for the Lorentz force:

$$\frac{1}{4\pi} \left(\boldsymbol{\nabla} \times \boldsymbol{B} \right) \times \boldsymbol{B} = -\boldsymbol{\nabla} \left(\frac{B^2}{8\pi} \right) + \frac{1}{4\pi} \left(\boldsymbol{B}.\boldsymbol{\nabla} \right) \boldsymbol{B} \qquad (2.10)$$

9

For the configuration chosen above, $\dfrac{\partial B_z}{\partial z} = 0$, then $(\boldsymbol{B}.\boldsymbol{\nabla})\,\boldsymbol{B} = 0$.

In this approximation, the MHD momentum equation becomes:

$$\rho\frac{\partial \boldsymbol{u}}{\partial t} + \rho\boldsymbol{u}.\boldsymbol{\nabla}\,\boldsymbol{u} = -\rho\boldsymbol{\nabla}\Phi - \boldsymbol{\nabla}\left(p + \frac{B^2}{8\pi}\right) \tag{2.11}$$

Implementing this equation is called the pseudo MHD code first introduced by A. P. Boss (1997). Here, the effect of magnetic field comes down to augmenting the gas pressure.

Note that the magnetic pressure is an exact representation of MHD effects for high conductivity and straight magnetic field lines. Detailed simulations (Fiedler & Mouschovias, 1993) have shown that initially straight magnetic field lines stay remarkably straight even when density increases by a factor of 10^6.

Having established the role of the magnetic field in supporting the cloud against gravitational collapse, one needs a parameter that measures whether the cloud can be supported by magnetic field or not. This parameter is the **mass-to-flux ratio** of the cloud.

For a sphere it is given by:

$$\frac{M}{\Phi} = \frac{M}{4\pi R^2 B_0} \tag{2.12}$$

where M is the mass of the cloud, Φ is the magnetic flux threading the cloud surface at radius R and B_0 is a uniform magnetic field.

There exists a critical mass-to-flux ratio below which the cloud is said to be magnetically supported. For a uniform spherical cloud this critical value takes the

form (Mestel, 1999), (Mac Low & Klessen, 2004):

$$\left(\frac{M}{\Phi}\right)_{crit} = \frac{2c_1}{3}\sqrt{\frac{5}{\pi G \mu_0}} \tag{2.13}$$

where G and μ_0 are the gravitational constant and the permeability of free space

respectively, and $c_1 \simeq 0.53$ is a numerically determined parameter

(Mouschovias & Spitzer, 1976).

If a cloud has a mass-to-flux ratio below this critical value, it is capable of

being supported by magnetic field. A frozen-in magnetic field would then prevent

collapse even if external pressure were to be infinite. A large external pressure would

only transform the cloud into a thin sheet with its plane perpendicular to the field

lines.(Mouschovias, 1991).

However, if the cloud's mass-to-flux ratio is above this critical value mag-

netic field alone is incapable to support it against gravitational collapse

(Mestel & Spitzer, 1956), (Mouschovias & Spitzer, 1976), (McKee, Zweibel, Good-

man, & Heiles, 1993).

The previous condition is a sufficient condition for collapse if the external

pressure is greater than the critical value:(Mouschovias, 1991)

$$P_{crit} = 1.89 \frac{c_s^8}{G^3 M^2 \left[1 - (M_{crit}/M)^2\right]^3} \tag{2.14}$$

Where $c_s = \left(\frac{kT}{\mu m_H}\right)^{1/2}$ is the isothermal speed of sound, k the Boltzmann constant, μ

the mean mass per particle in units of the atomic hydrogen mass m_H (Mouschovias,

1987).

For any given mass-to-flux ratio of a cloud, one can find the initial value of the magnetic field B_0 using the following equation (Price & Bate, 2007):

$$B_0 = 814\mu G \left(\frac{M}{\Phi}\right)^{-1} \left(\frac{M}{1M_\odot}\right) \left(\frac{R}{0.013pc}\right)^{-2} \qquad (2.15)$$

2.2.1 Magnetic diffusion

A rough estimate of the magnetic field flux in a cloud's core and in a newborn star show that the magnetic flux should be reduced by several orders of magnitude (Inutsuka, 2012).

Although it is difficult to measure the field strength in dense molecular cloud cores, various Zeeman effect based observations indicate that the cores, with typical radius of $0.01pc \approx 10^{16}cm$, have a magnetic field of at least $10\mu G$ (Crutcher, 1999), (Crutcher, Hakobian, & Troland, 2009). Thus, its magnetic flux can be estimated as:

$$\Phi_{core} \sim B_{core}R^2{}_{core} \sim 10\mu G \times \left(10^6 cm\right)^2 = 10^{27}Gcm^2 \qquad (2.16)$$

In contrast, the observed field strengths of young stellar objects, with typical radius of $10^{11}cm$, are reported to be at most of the order of kG (Inutsuka, 2012). Thus, the magnetic flux of the star should be smaller than the following estimate:

$$\Phi_* \sim B_*R_*{}^2 \sim kG \times \left(10^{11}cm\right)^2 = 10^{25}Gcm^2 \qquad (2.17)$$

This means, that through the star formation process, the cloud's core must have lost magnetic flux. Thus, the question arises: how to reduce the magnetic flux in a protostar?

The diffusion of the magnetic field in a weakly ionized gas can be considered as the result of various effects.

1. Ambipolar diffusion: This effect takes place in the limit of low ionization. In this case, the magnetic field is frozen into the charged species only and it drifts along with them through the neutrals.

2. Resistive diffusion: In this limit the ionization is high and the charged particles are completely decoupled from the field by collisions with neutrals (Wardle, 2004).

Since the medium of interest has low ionization fraction, the ambipolar diffusion scenario may be dominant. And this process will be explained in the following section.

2.3   Ambipolar diffusion

2.3.1   Basic process

The magnetic field plays an important role during the process of star formation, in particular during its initial phase. It is likely to control the onset of collapse.

The free fall time scale for a pressureless cloud to collapse from rest is well known to be :

$$t_{ff} = \left(\frac{3\pi}{32G\rho} \right)^{1/2} \tag{2.18}$$

In a dense core, $t_{f}f \approx 10^3 yr$, which is relatively short by astronomical standard (Crutcher, 1999). So a magnetized cloud is supported against collapse, which makes the timescale of the collapse longer than the t_{ff}. As it has been mentioned in the previous section, a frozen-in magnetic field increases the gas pressure, and if the magnetic field does not decay, a stable cloud will remain stable. But is it possible for a previously stable cloud to collapse? In other words, could a subcritical cloud become supercritical? The answer is yes, and it is related to ambipolar diffusion.

Charged particles like electrons or ions are tied to the magnetic field lines by the Lorentz force, but neutrals are not affected directly. Given that dense molecular cores are dominated by neutrals because of lack of ionization, how can a magnetic field have a significant effect on the collapse? This is possible through collisions between the neutrals and ions (electrons do not play a significant role). In low ionization region, the charged particles do not collide sufficiently with the neutrals in order to keep them locked to the magnetic field. As a result the ions remain frozen into the magnetic field lines, while the neutrals drift away from them. In the neutrals rest frame, the ions appear drifting away to the periphery along with the field lines. This drift between the ions and neutrals in called "ambipolar diffusion".

Now the question remains, how does this drift between the ions and neutrals allow a subcritical cloud to collapse? When neutrals migrate into the center of the cloud, the mass is going from the peripheral tubes to the central flux tubes. This is why ambipolar diffusion is said to redistribute the mass in the flux tubes. When the mass in the central flux tubes increases, a central core forms with increasing mass-to-flux ratio. This leads to the collapse of the core.

In the previous subsection, we mentioned that ambipolar diffusion is a mechanism for the cloud to lose magnetic support. This occurs when the neutrals move toward the center, and leave behind the ions along with the magnetic field lines. Then, in the neutral supercritical core that would eventually collapse, the magnetic flux is smaller than that in the initial cloud.

2.3.2   Ambipolar diffusion timescale

From the previous discussion, the ambipolar diffusion timescale is expected to depend on the ionization of the cloud and the magnetic field.

To find the ambipolar diffusion timescale, one needs to find the drift velocity between the ions and neutrals. In a first consideration this can be done by neglecting the ion's pressure and momentum compared to that of the neutral species. In this case, the Lorentz force $\boldsymbol{F}_L$ exerted on the ions is in equilibrium with the drag force $\boldsymbol{F}_d$ exerted by the neutrals. On one hand, the Lorentz force is the driving force leading the ions to travel through the "sea" of neutrals. This motion achieves a terminal velocity owing to the balance between the Lorentz force and the drag force. Therefore, we

have the following equations:

$$\frac{1}{4\pi} \left(\boldsymbol{\nabla} \times \boldsymbol{B} \right) \times \boldsymbol{B} = \gamma \rho_n \rho_i \left(\boldsymbol{u}_i - \boldsymbol{u}_n \right) \tag{2.19}$$

where $\gamma = 3.5 \times 10^{13} cm^3 g^{-1} s^{-1}$ is the drag coefficient.

Then, the drift velocity becomes:

$$\boldsymbol{u}_D = \boldsymbol{u}_i - \boldsymbol{u}_n = \frac{1}{4\pi\gamma\rho_n\rho_i} \left(\boldsymbol{\nabla} \times \boldsymbol{B} \right) \times \boldsymbol{B} \tag{2.20}$$

Considering due to symmetry the drift occurring across a cylindrical region of radius R, with a typical bend in the field of order R, the Lorentz force becomes:

$$\frac{1}{4\pi} \left(\boldsymbol{\nabla} \times \boldsymbol{B} \right) \times \boldsymbol{B} = \frac{B^2}{4\pi R} \tag{2.21}$$

Then, the ambipolar diffusion timescale t_{AD} is given by (Mac Low & Klessen, 2004)

$$t_{AD} = \frac{R}{\boldsymbol{u}_D} = \frac{4\pi\gamma\rho_i\rho_n R}{\left(\boldsymbol{\nabla} \times \boldsymbol{B} \right) \times \boldsymbol{B}} \approx \frac{4\pi\gamma\rho_i\rho_n R^2}{B^2} \tag{2.22}$$

Or:

$$t_{AD} = (25 Myr) \left(\frac{B}{3\mu G} \right)^{-2} \left(\frac{n}{10^2 cm^{-3}} \right)^2 \left(\frac{R}{1pc} \right)^2 \left(\frac{x_i}{10^{-6}} \right) \tag{2.23}$$

Where B is the magnetic field, n is the number density of the neutrals, R is the radius of the clouds and x_i is the degree of ionization.

This equation shows that the timescale of ambipolar diffusion is proportional to the degree of ionization. So, a smaller degree of ionization leads to a shorter ambipolar

diffusion timescale. Since the ionization in the center of the cloud is smaller than the ionization in the envelope, ambipolar diffusion becomes more important in the core of the cloud. Therefore, the core of a cloud could undergo gravitational collapse while the envelope remains stable. Equation (2.23) shows that ambipolar diffusion is significant when the initial magnetic field is large. And, a smaller radius leads to faster drift, which supports the view that only the core would collapse instead of the whole cloud.

The ambipolar diffusion timescale is usually expressed in units of the free fall timescale t_{ff}. It is given by (A. P. Boss, 1997):

$$\frac{t_{AD}}{t_{ff}} \approx 9 \left(\frac{L}{0.1pc} \right)^2 \left(\frac{n}{10^3 cm^{-3}} \right)^{3/2} \left(\frac{x_i}{10^{-7}} \right) \tag{2.24}$$

where L is the tenth of the cloud's radius, n the number density of the neutral atoms and x_i the degree of ionization.

For $L = 0.0010pc$, $n = 4 \times 10^6 cm^{-3}$, and $x_i = 10^{-7}$, used in our thesis, the timescale of ambipolar diffusion becomes $t_{AD} \approx 200.t_{ff}$.

This is in contrast to the typical value of ambipolar diffusion timescale $t_{AD} = 10t_{ff}$. If the timescale of ambipolar diffusion is significantly longer than the free fall timescale, how can this process still be relevant to star formation?

The view was that the process of ambipolar diffusion was only important when its timescale is comparable to the free-fall time (Nakano & Tademaru, 1972). But, when magnetic field is taken into consideration, the free fall timescale is not the relevant timescale to consider. In this case, ambipolar diffusion should be compared to the

timescale of the formation of a protostar starting from a coreless cloud (Mouschovias et al., 2006).

For a significant magnetic field support, $B = 1600\mu G$, the ambipolar diffusion timescale is as short as $t_{AD} \approx 2Myr$. So, for clouds with ages of a few million years, ambipolar diffusion is relevant to star formation. (No cloud with similar magnetic field strength were observed.)

2.4 Objections on the standard theory

Although previous observations (Greaves & Holland, 1999) have found that ion neutral drift indeed occurs in molecular clouds. The most recent observations (Crutcher, 2012) seem not to support the role of ambipolar diffusion in molecular clouds. This author suggests the magnetic field dominates turbulence in molecular clouds but there were no definitive evidence that it dominates gravity nor for ambipolar-diffusion-driven star formation. Despite his observations, Crutcher admitted that his astrophysical conclusions remain tentative, so that more investigation on ambipolar diffusion remains an interesting topic.

Ambipolar diffusion predicts that the mass-to-flux-ratio of the core of the cloud increases compared to that of the envelope.
We define $\mathcal{R} = \dfrac{[M/\Phi]_{core}}{[M/\Phi]_{env}}$.
The ambipolar diffusion theory of core formation requires $\mathcal{R}$ to be approximately equal to the inverse of the original subcritical $\dfrac{M}{\Phi}$, or at least $\mathcal{R} > 1$.
Normally observation of magnetic field is tricky. A line of sight measurement based

on the Zeeman effect yields only an upper limit. Therefore one has to determine the angle between the magnetic field vector and the line of sight in order to get the reasonable value of the magnetic field.

But testing ambipolar diffusion is relatively easier, because all one has to determine is the change in $\dfrac{M}{\Phi}$ from an envelope region to a core region of a cloud whose contraction was driven by ambipolar diffusion. Thus, the exact value of the magnetic field isn't necessary for such a test.

In order for ambipolar-diffusion theory to pass the test, the value of $\mathcal{R}$ found should be above 1.

Four dark clouds had strong detected B_{LOS} in the Troland & Crutcher OH Zeeman survey (Troland & Crutcher, 2008). $\mathcal{R}$ was measured for these clouds (Crutcher et al., 2009). The results were:

$\mathcal{R}\left(L1448CO\right) = 0.02 \pm 0.36$, $\mathcal{R}\left(B217 - 2\right) = 0.15 \pm 0.43$, $\mathcal{R}\left(L1544\right)) = 0.42 \pm 0.46$ and $\mathcal{R}\left(B1\right) = 0.41 \pm 0.20$.

Hence, $\mathcal{R} < 1$ in all four cases and the result didn't match the ambipolar diffusion prediction.

This result means that the mass-to-flux ratio increases in the envelope compared to that of the core, implying that the magnetic field strength decreases and the magnetic flux is lost. Crutcher (2012) suggested that this could be due to magnetic reconnection (Lazarian, 2005), which is a sort of speculation and needs to be verified.

Another theoretical prediction of ambipolar diffusion is the scaling of the magnetic field in terms of the density. The magnetic field may be parameterized as

a function of density as (A. P. Boss, 1997) :

$$B = B_0 \left(\frac{\rho}{\rho_0} \right)^{\kappa} \tag{2.25}$$

which holds in the envelope of the cloud, where B_0 is a scaling time-dependent factor, ρ_0 is the initial density, and ambipolar diffusion predicts that κ is between $1/2$ and $1/3$.

Based on the most recent observational review on magnetic fields in molecular clouds by Crutcher (2012), the power-law exponent is $2/3$ for number densities $n_H \gtrsim 300 cm^{-3}$.

Another objection against ambipolar diffusion is that it distinguishes between the formation of low-mass and high-mass stars. The standard theory suggested that low-mass stars form from low-mass magnetically subcritical cores, whereas high-mass stars and stellar clusters form from magnetically supercritical cloud cores (Shu, Adams, & Lizano, 1987), (Lizano & Shu, 1989). According to Mac Low and Klessen (2004), interstellar turbulence may unify both descriptions of star formation. This issue is still controversial.

Chapter 3

Formulation of the problem

3.1 Equations of magneto-hydro-dynamics (MHD)

First we present the set of equations of the non-ideal MHD, which will be later simplified to match our calculations.

In a single fluid approximation, the equations are:

$$\frac{\partial \rho}{\partial t} + \boldsymbol{\nabla}.\left(\rho\boldsymbol{u}\right) = 0 \qquad (3.1)$$

$$\frac{\partial \boldsymbol{u}}{\partial t} + \boldsymbol{u}.\boldsymbol{\nabla}\boldsymbol{u} = -\boldsymbol{\nabla}\Phi - \frac{1}{\rho}\boldsymbol{\nabla}P + \frac{1}{\rho}\left(\boldsymbol{\nabla}\times\boldsymbol{B}\right)\times\boldsymbol{B} \qquad (3.2)$$

$$\frac{\partial \boldsymbol{B}}{\partial t} - \boldsymbol{\nabla}\times\left(\boldsymbol{u}_n\times\boldsymbol{B}\right) = \boldsymbol{\nabla}\times\left\{\left[\eta_{AD}\left(\boldsymbol{\nabla}\times\boldsymbol{B}\right)\times\boldsymbol{B}\right]\times\boldsymbol{B} - \eta\boldsymbol{\nabla}\times\boldsymbol{B}\right\} \qquad (3.3)$$

$$\boldsymbol{\nabla}.\boldsymbol{B} = 0 \qquad (3.4)$$

where ρ and $\boldsymbol{u}$ are the density and velocity of the neutrals, Φ is the gravitational potential, P the gas pressure, and $\boldsymbol{B}$ is the magnetic field. We omit the index n because the ions are not taken into consideration.

To get Φ, the Poisson's equation is added:

$$\nabla^2 \Phi = 4\pi\rho \tag{3.5}$$

Furthermore, an equation of state should be added. An isothermal equation of state can be used given by:

$$P = c_s^2 \rho \tag{3.6}$$

with c_s is the isothermal speed of sound, temperature dependent (see Eq. 2.14)).

When ionization is taken into account, the right hand side of the continuity equation (Eq. (3.1)) is not zero. Instead, a source term should be included which is according to Brandenburg and Zweibel (1995):

$$\frac{\partial \rho}{\partial t} + \boldsymbol{\nabla}.\left(\rho \boldsymbol{u}_n\right) = -\zeta\rho + \alpha\rho_i^2 \tag{3.7}$$

where ζ is the ionization coefficient and α is the recombination coefficient.

The effect of the term on the right hand side is that it describes the residual density of the neutrals.

The single fluid approach can be justified physically. In molecular clouds the pressure and momentum of the ions can be neglected compared to those of the neutrals. Under these conditions, the Lorentz Force exerted on ions is balanced by the drag force exerted on neutrals. This is the case of strong coupling between the neutrals and the field lines. Thus, the plasma is reasonably described by a single fluid of neutral density $\rho_n >> \rho_i$ where ρ_i is the ion density (Shu et al., 1987) (Choi &

Wiita, 2009) ; (Kim, 2011).

The single fluid approach is a possible treatment and it has been widely used in modeling the ambipolar diffusion (Kudoh et al. 2007)

On the other hand, the two-fluid approach has been suggested to describe the case when a molecular cloud would have a neutral fluid collapsing inward with respect to an ionized fluid locked to magnetic field.

Indeed, the two-fluid approach is more realistic to describe ambipolar diffusion. It is certainly more complicated approach and beyond the scope of the present thesis, and is worth investigating in future work.

In the following, we present a simplified version of the non-ideal MHD equation which we have used to obtain the result described in chapter 5 of this thesis.

3.2   The non-ideal induction equation

It is instructive to derive the induction equations taking into account resistive effects, such as Ohmic resistivity and ambipolar diffusion.

Starting with the Ampere's law and the Faraday's law, one has:

$$\boldsymbol{J} = \frac{1}{\mu} \boldsymbol{\nabla} \times \boldsymbol{B} \tag{3.8}$$

$$\frac{\partial \boldsymbol{B}}{\partial t} = -\boldsymbol{\nabla} \times \boldsymbol{E} \tag{3.9}$$

$$\boldsymbol{J} = \sigma \left(\boldsymbol{E} + \boldsymbol{u}_i \times \boldsymbol{B} \right) \tag{3.10}$$

where μ is the permeability, σ is the conductivity and $\boldsymbol{u}_i$ is the ions velocity.

If the electrical conductivity is high in a molecular clouds, then the Ampere's law is valid for a long time scale process like the ambipolar diffusion (see appendix A). The electric field can be obtained from equation (3.10):

$$\boldsymbol{E} = \frac{1}{\sigma} \left(\boldsymbol{J} - \boldsymbol{u}_i \times \boldsymbol{B} \right) \tag{3.11}$$

Inserting Eqs.(3.8) and (3.11) into Eq. (3.9) leads to the induction equation:

$$\frac{\partial \boldsymbol{B}}{\partial t} = \boldsymbol{\nabla} \times \left(\boldsymbol{u}_i \times \boldsymbol{B} - \eta \boldsymbol{\nabla} \times \boldsymbol{B} \right) \tag{3.12}$$

where $\eta = \dfrac{1}{\mu\sigma}$ is the magnetic diffusivity (or Ohmic resistivity).

Assuming η to be constant leads to:

$$\frac{\partial \boldsymbol{B}}{\partial t} = \boldsymbol{\nabla} \times \left(\boldsymbol{u}_i \times \boldsymbol{B} \right) - \eta \left(\nabla^2 \boldsymbol{B} - \boldsymbol{\nabla} \left(\boldsymbol{\nabla}.\boldsymbol{B} \right) \right) \tag{3.13}$$

Using $(\boldsymbol{\nabla}.\boldsymbol{B} = 0)$ leads to:

$$\frac{\partial \boldsymbol{B}}{\partial t} = \boldsymbol{\nabla} \times \left(\boldsymbol{u}_i \times \boldsymbol{B} \right) - \eta \nabla^2 \boldsymbol{B} \tag{3.14}$$

The first term on the right-hand side of this equation represents *advection* , while the second term is a *diffusion term.*

In Eq. (2.20), the drift velocity was introduced as $\boldsymbol{u}_D = \boldsymbol{u}_i - \boldsymbol{u}_n$. This replaces the ion velocity from the induction equation (Brandenburg & Zweibel, 1994); which

becomes:

$$\frac{\partial \boldsymbol{B}}{\partial t} = \boldsymbol{\nabla} \times (\boldsymbol{u}_n \times \boldsymbol{B} + \boldsymbol{u}_D \times \boldsymbol{B} - \eta \boldsymbol{\nabla} \times \boldsymbol{B}) \tag{3.15}$$

Inserting Eq. (2.20) into this equation, one obtains an induction equation of the following form:

$$\frac{\partial \boldsymbol{B}}{\partial t} - \boldsymbol{\nabla} \times (\boldsymbol{u}_n \times \boldsymbol{B}) = \boldsymbol{\nabla} \times \left[\frac{(\boldsymbol{\nabla} \times \boldsymbol{B}) \times \boldsymbol{B}}{4\pi\gamma\rho_i\rho_n} \times \boldsymbol{B} - \eta \boldsymbol{\nabla} \times \boldsymbol{B} \right] \tag{3.16}$$

Let $\eta_{AD} = \dfrac{1}{4\pi\gamma\rho_i\rho_n}$ be the ambipolar diffusion coefficient (Brandenburg & Zweibel, 1994).

Finally, the induction equation including the effects of both Ohmic and ambipolar diffusion:

$$\frac{\partial \boldsymbol{B}}{\partial t} - \boldsymbol{\nabla} \times (\boldsymbol{u}_n \times \boldsymbol{B}) = \boldsymbol{\nabla} \times \left\{ [\eta_{AD} (\boldsymbol{\nabla} \times \boldsymbol{B}) \times \boldsymbol{B}] \times \boldsymbol{B} - \eta \boldsymbol{\nabla} \times \boldsymbol{B} \right\} \tag{3.17}$$

3.3 Estimates of the resistive effects

The resistive effects introduced in the set of non ideal MHD above are the ambipolar diffusion and the Ohmic resistivity. In this paragraph, we first check the dimensions of the terms, then estimate their numerical values, and finally decide whether or not this system of equations to solve could reduce to ideal MHD in we are adapting.

We begin with the dimensional analysis, and the dimensions of the diffusion terms in Eq.(3.17) should be consistent with that of $\dfrac{\partial \boldsymbol{B}}{\partial t} = \dfrac{[B]}{[T]}$.

The ambipolar diffusion term from equation (3.17) is $\boldsymbol{\nabla} \times [\eta_{AD} (\boldsymbol{\nabla} \times \boldsymbol{B}) \times \boldsymbol{B}] \times \boldsymbol{B}$.

As seen in Eq. (2.20), its dimension is:

$$dim\,[\eta_{AD}\,(\boldsymbol{\nabla} \times \boldsymbol{B}) \times \boldsymbol{B}] = dim\,(\boldsymbol{u}_D) \tag{3.18}$$

So, the dimensions of the ambipolar diffusion term are:

$$dim\,(\boldsymbol{\nabla} \times [\eta_{AD}\,(\boldsymbol{\nabla} \times \boldsymbol{B}) \times \boldsymbol{B}] \times \boldsymbol{B}) = \frac{1}{[L]}\frac{[L]}{[T]}\,[B] = \frac{[B]}{[T]} \tag{3.19}$$

Q.E.D

From Eqs. (3.8) and (3.10), respectively:

$$[\mu] = \frac{[B]}{[L]\,[J]} \tag{3.20}$$

$$[\sigma] = \frac{[J]\,[T]}{[L]\,[B]} \tag{3.21}$$

We hence deduce the dimensions of the magnetic diffusivity:

$$[\eta] = \frac{[B]}{[L]\,[J]}\frac{[J]\,[T]}{[L]\,[B]} = \frac{[L]^2}{[T]} \tag{3.22}$$

So, the dimensions of the Ohmic resistivity term are:

$$dim\,(\boldsymbol{\nabla} \times (\eta \boldsymbol{\nabla} \times \boldsymbol{B})) = \frac{1}{[L]}\frac{[L]^2}{[T]}\frac{[B]}{[L]} = \frac{[B]}{[T]} \tag{3.23}$$

Q.E.D.

After proving that the two terms have the same dimensions as the change of B with respect to time, we will calculate their maximal numerical values for our models.
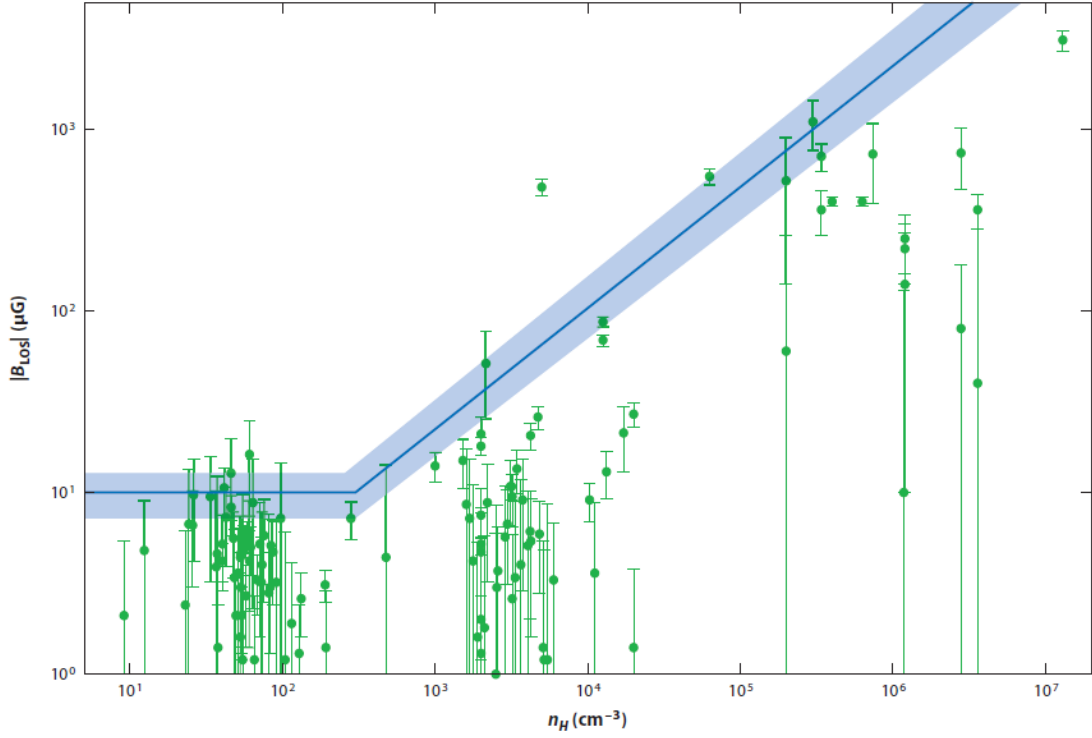
Figure 6

The set of diffuse cloud and molecular cloud Zeeman measurements of the magnitude of the line-of-sight component B_{LOS} of the magnetic vector **B** and their 1σ uncertainties, plotted against $n_H = n(\text{HI})$ or $2n(H_2)$ for HI and molecular clouds, respectively (Crutcher et al. 2010). Although Zeeman measurements give the direction of the line-of-sight component as well as the magnitude, only the magnitudes are plotted. The solid blue line shows the most probable maximum values for $B_{TOT}(n_H)$ determined from the plotted values of B_{LOS} by the Bayesian analysis of Crutcher et al. (2010). Also shown (plotted as *light blue shading*) are the ranges given by acceptable alternative model parameters to indicate the uncertainty in the model.

Figure 3.1: Line of sight magnetic field strength and maximum total magnetic field strength as a function of the neutrals number densities. Taken from Crutcher (2012)

Crutcher (2012) plotted the magnitude of the line-of-sight component B_{LOS} of the magnetic vector **B** against the number densities of the neutrals (see figure 3.1). Also, this figure shows the most probable maximum values for B_{TOT}.

In our calculation, we consider a neutral number density $n_H = 10^5 cm^{-3}$. According to Fig. (3.1), the maximum magnetic field is a few hundreds of microGauss. So the

maximum magnetic field strength we used in our simulations is $B = 400\mu G$. The radius of the sphere is $R = 0.010pc = 3.0857 \times 10^{16}cm$.

The ambipolar diffusion term can be approximated by:

$$\boldsymbol{\nabla} \times [\eta_{AD} \left(\boldsymbol{\nabla} \times \boldsymbol{B}\right) \times \boldsymbol{B}] \times \boldsymbol{B} \approx \frac{1}{4\pi\gamma\rho_i\rho_n} \frac{B^3}{R^2} \tag{3.24}$$

For our models, the neutral density is $\rho_n = \mu n_n m_H = 3.3471 \times 10^{-20}g.cm^{-3}$, the degree of ionization is $x_i = \dfrac{n_i}{n_n} = 10^{-7}$. The mass of the ions is $m_i = 10m_n$, so the ion density becomes $\rho_i = m_i n_i = 10 m_n x_i n_n = 10^{-6}\rho_n$. Then:

$$\frac{1}{4\pi\gamma\rho_i\rho_n} \frac{B^3}{R^2} = \frac{10^6}{4\pi\gamma\rho_n^2} \frac{B^3}{R^2} \approx 1.5903 \times 10^{-17}G/s \tag{3.25}$$

The Ohmic resistivity term:

$$\boldsymbol{\nabla} \times (\eta\boldsymbol{\nabla} \times \boldsymbol{B}) \approx \frac{B}{\eta R^2} \tag{3.26}$$

where $\eta = \dfrac{1}{\mu\sigma}$, and with T=10K in Eq. (A.3) we find $\sigma = 3.0826 \times 10^{10}$. Then $\eta = 2.5815 \times 10^{-12}$.

$$\frac{B}{\eta R^2} = 1.0845 \times 10^{-48}G/s \tag{3.27}$$

Therefore, for the density and magnetic field of interest, the Ohmic resistivity term is clearly negligible compared to the ambipolar diffusion term. But the latter is also very small, and to computer precision it could be safely considered zero.

Since these two terms can be approximated by zero, the non-ideal induction equation

reduces to:

$$\frac{\partial \boldsymbol{B}}{\partial t} - \boldsymbol{\nabla} \times (\boldsymbol{u}_n \times \boldsymbol{B}) = 0 \tag{3.28}$$

This is the ideal induction equation. We will solve this equation, along with the equations (3.1), (3.2), (3.4) and (3.5). These equations are called the ideal MHD equations.

3.4 Chemical cloud composition

Ionization process in molecular clouds are expected to be less effective. The estimated value of the degree of ionization is about $10^{-7}s^{-1}$. Based on available data, Spitzer and Tomasko (1968) obtained for the ionization rate (ζ) of hydrogen atoms a probable lower limit of $6.7 \times 10^{-18}s^{-1}$ and a probable upper limit of $1.2 \times 10^{-15}s^{-1}$.

More recently, Webber (1998) estimated minimum ionization rate of $(3-4) \times 10^{-17}s^{-1}$ for H atoms, and pointed out the possibility of enhanced rates exceeding $10^{-16}s^{-1}$ near massive stars with strong stellar winds.

No definitive value for dense clouds emerges from the various studies, but it seems that a value of $1 \times 10^{-17}s^{-1}$ is too small and 5×10^{-17} or even 1×10^{-16}, may be a more realistic mean value (Dalgarno, 2006).

Cosmic rays are the primary cause of ionization in molecular cloud cores. Their energies range from MeV to ultrarelativistic values, but the rays that mostly ionize the interstellar medium are those with energies smaller than 1 GeV (Viti, Hartquist, Bell, Williams, & Banerji, 2013). These particles are capable of entering

the cloud's envelope and ionizing Hydrogen in the core. Ultraviolet photoioniza-tion is practically shielded and is not very significant when it comes to the core's ionization.

Over the range of densities of interest ($10^3 - 10^6 cm^{-3}$), the number of ions can be approximated by a power law (Fiedler & Mouschovias, 1992):

$$n_i = K_{CR} \left(\frac{n_n}{10^5 cm^{-3}} \right)^{1/2} \tag{3.29}$$

where $K_{CR} \approx \left(\frac{10^5 \zeta}{\alpha_{dr}} \right)^{1/2}$, ζ is the cosmic ray ionization coeeficient, and $\alpha_{dr} = 2.0 \times 10^{-7} \left(\frac{T}{300K} \right) s^{-1}$ is the dissociative coeeficient. Even though the UV ionization is negligible in the central of the cloud, it is possible for it to penetrate into the cloud and directly ionize atomic species such as sulfur, iron, silicon, carbon, and magnesium greatly increasing the ionization in the low-density envelope. Thus, a very small correction term to the equation above is needed to take UV ionization into account. That finally gives the number density of ionized particles (Fiedler & Mouschovias, 1992):

$$n_i = K_{CR} \left(\frac{n_n}{10^5 cm^{-3}} \right)^{1/2} + K_{UV} \left(\frac{10^3 cm^{-3}}{n_n} \right)^2 \tag{3.30}$$

where

$$K_{CR} = 1, 3 \quad or \quad 5 \times 10^{-3} cm^{-3}$$

$$K_{UV} = 4.68 \times 10^{-4} cm^{-3}$$

As discussed in the previous section, in the range of the density and magnetic field strengths of interest the resistive terms are negligible. Hence, the use of ideal MHD is justified.

In the ideal MHD approach, the magnetic flux is constant and the ionization does not come into play. In contrast, in the non-ideal approach, the ionization plays a decisive role in star formation, and namely in the ambipolar diffusion process (see section (2.3.2)).

So, the ionization has been so far discussed qualitatively, its effect on the ambipolar diffusion timescale was explained. Henceforth, the ionization will not be included in the numerical work because the ideal MHD will be used. Implementing non-ideal set of equations, taking into account the ionization, heating and cooling processes is worth investigating in future work.

Chapter 4

The cloud models

In this chapter, we introduce the initial conditions used to explore the collapse of a magnetized rotating cloud. We firstly describe a spherical cloud with uniform density to which a small perturbation is introduced. Then, two different shapes of centrally condensed clouds are studied: the flattened sphere, and the exponentially decreasing density profile. Finally, we describe the method of calculations used to investigate the problem.

For all models, the clouds are taken to be in a solid body rotation, the mass of the clouds is fixed to one solar mass ($M = M_\odot$) and the initial temperature is set to $T_i = 10K$. The solid body rotation is only considered for simplicity. A molecular cloud is likely to have a differential rotation.

The parameters are the density ρ and angular velocity Ω. They are often replaced by the parameters α and β, which are the ratios of thermal and rotational energies

to the gravitational energy, respectively.

$$\alpha = \left| \frac{E_{thermal}}{E_{gravitational}} \right| \qquad (4.1)$$

$$\beta = \left| \frac{E_{rotational}}{E_{gravitational}} \right| \qquad (4.2)$$

The magnetic field is also presented by the parameter mass-to-flux ratio $\frac{M}{\Phi}$. These parameters are easily found for a uniform spherical cloud, but hard to find for the other density profiles.

4.1 Uniform density

For the sake of comparison, we reproduce the model by A. Boss and Keiser (2013) (hereafter BK13) which was based on MHD calculations assuming a sphere of uniform density. The model was originally proposed by Boss and Bodenheimer (A. Boss & Bodenheimer, 1979) (hereafter BB79) and studied neglecting the effect of magnetic field. This work is considered interesting because we monitor more closely the effect of magnetic field not only on the collapse of the cloud itself, but also on the shape of the cloud during the collapse and the magnetic braking effect that arises due to the magnetic field and rotation.

The cloud in this section has a uniform spherical density. It has a solar mass $M = 1.0 M_{\odot}$ and radius $R = 3.2 \times 10^{16} cm = 0.010 pc$. The cloud is assumed to be in solid body rotation around the $\widehat{z}-axis$ with angular velocity $\Omega_i = 1.6 \times 10^{-12} rad.s^{-1}$. The initial neutral Hydrogen density is $\rho_0 = 1.44 \times 10^{-17} g.cm^{-3}$, the ratio of the

cloud's density to the medium density is 144:1. The mean molecular weight is taken to be equal to 2, reflecting composition of Z=N (equal protons and neutrons).

To make sure that the initial values are consistent with observations, we calculate the gravitational energy, the thermal energy and the rotational energy of the cloud. These energies are given by:

$$E_{grav} = -\frac{3}{5}\frac{GM^2}{R} \tag{4.3}$$

$$E_{th} = \frac{3}{2}Nk_BT \tag{4.4}$$

$$E_{rot} = \frac{1}{5}MR^2\Omega^2 \tag{4.5}$$

where $N = \dfrac{M}{m_u\mu}$, m_u the atomic mass unit and Ω is the cloud's angular velocity. Taking the ratio of thermal to gravitational energy to be α, and that of the rotational to gravitational energy to be β, and with the initial values above, one finds $\alpha_i = 0.2179$ and $\beta_i = 0.20$, consistent with values inferred from observations. Magnetic field will be chosen to be parallel or perpendicular to the axis of rotation, oriented along the $\hat{z}-axis$ or $\hat{x}-axis$. We chose these two directions in order to obtain single or multiple system instead of a disk. An arbitrary angle could have been chosen between them,and this is called "Magnetic Field-Rotation Misalignment". Li, Krasnopolsky, and Shang (2013) confirmed the basic result of Joos, Hennebelle, and Ciardi (2012) that the misalignment between the magnetic field and the axis of rotation of the cloud is indeed conducive to disk formation. This is why we chose the magnetic field parallel and perpendicular to the axis of rotation. Crutcher (2012) plotted the line of sight component of the magnetic field as a func-

tion of the neutral number density. So the values chosen throughout this work fulfills two requirements:

1. The magnetic field strength is below the maximum value plotted in Crutcher (2012) for the corresponding neutral density (see Fig. (3.1)).

2. The magnetic field strength is low enough for the ambipolar diffusion term (see section (3.3)) to remain small so that an ideal MHD approach can be used.

Starting with a sphere of uniform density, a perturbation is needed to trigger the collapse of the cloud. In BB79, the initial density perturbation is azimuthal, of the second order and of amplitude 0.5. In our work, we take a smaller amplitude of 0.1. The perturbation introduced to the initially uniform density reads:

$$\delta\rho = 0.1 cos(2\phi) \tag{4.6}$$

Thus, the initial perturbed density becomes:

$$\rho = \rho_0(1 + \delta\rho) = \rho_0\left(1 + 0.1 cos(2\phi)\right) \tag{4.7}$$

The equation of state is taken to be isothermal (Eq. (3.6)).

Finally, the boundary conditions are chosen to be periodic on each face of the grid's cubic box.

4.2 Centrally condensed clouds

4.2.1 Flattened sphere density profile

Observational evidence shows that pre-stellar cores do not posses uniform densities (Froebrich, 2015). Rather the density increases towards the center and reach a plateau. Analytically such functions can be described by:

$$\rho = \rho_0 \left[\frac{R_0}{\left(R_0{}^2 + r^2\right)^{1/2}} \right]^{\eta} \tag{4.8}$$

where ρ_0 is the central density, R_0 is a free parameter. For $\eta = 5$, this gives the classical Plummer sphere and $\eta = 4$ was used by Whitworth and Ward-Thompson (2001). For our model we will use $\eta = 2$, so that the density profile reduces to:

$$\rho = \rho_0 \left[\frac{R_0^2}{\left(R_0{}^2 + r^2\right)} \right]$$

$$\rho = \frac{\rho_0}{1 + \left(\dfrac{r}{R_0}\right)^2} \tag{4.9}$$

This is the non singular version of the power law density distribution where $\rho \propto r^{-2}$. For the power law profile, the density is infinite for r=0, which is not a physical limit. We consider a central density 10 times bigger than the density at the boundary, and

we find the parameter R_0:

$$\rho_0 = 10\frac{\rho_0}{1 + \left(\dfrac{R}{R_0}\right)^2} \tag{4.10}$$

$$R_0 = \frac{R}{3} \tag{4.11}$$

Hence, the initial density is taken to be:

$$\rho_i = \frac{\rho_0}{1 + \left(\dfrac{3r}{R}\right)^2} \tag{4.12}$$

where ρ_0 is the density at the center of the cloud and R is the radius of the cloud. Two values for the initial densities are considered $\rho_0 = 1.8 \times 10^{-18} g.cm^{-3}$ and $\rho_0 = 3.1 \times 10^{-17} g.cm^{-3}$. And the radius of the cloud is chosen to be $R = 0.07pc$. We introduce to this cloud a density perturbation similar to that introduced to the uniform density (see Eq. 4.6).

The cloud is considered to be in solid body rotation around the $\widehat{z}$-direction with two values for the angular velocity: $\Omega_0 = 2.9 \times 10^{-13} rad.s^{-1}$ and $\Omega_0 = 2.9 \times 10^{-15} rad.s^{-1}$. The first one represents a fast rotating cloud and the second is a slowly rotating cloud. As for the magnetic field, we will deal with three values $B_0 = 0, 10\mu G$ and $100\mu G$, parallel to the axis of rotation.

Although it was straightforward to calculate the energies in Eqs.(4.3), (4.4) and (4.5), it is very difficult to calculate them for this density profile. So the numerical values of the radius and angular velocities were chosen empirically for this model.

The radius is big enough to clearly show the density profile, and the angular velocity was chosen small so that the cloud would be slowly rotating.

We will solve the MHD set of equation with a barotropic equation of state:

$$P = K\rho^{\gamma} \tag{4.13}$$

where $\gamma = 1$, $K = c_s{}^2$ for $\rho < \rho_c$ (isothermal calculations),

and $\gamma = 7/5$, $K = c_s{}^2\rho_c^{-2/5}$ for $\rho > \rho_c$.

A critical density $\rho_c = 10^{-14}gcm^{-3}$ is branching the two descriptions.

We note that in case of $\rho > \rho_c$, the cloud becomes optically thick (or opaque) to infrared radiation, so that its temperature starts rising upon compression. This equation of state is more realistic than the one used in the uniform model above, because it mimics the non-isothermal effects of the cloud and also the radiative transfer (A. Boss & Keiser, 2013).

4.2.2 Exponential density profile

We also consider the density profile described the exponential profile. This will be intermediate between the two options described above. and the flattened sphere, the initial density profile is chosen to be:

$$\rho_i = \rho_0 exp\left[-\left(\frac{r}{R_0}\right)^2\right] \tag{4.14}$$

where ρ_0 is the central density, R_0 is a free parameter.

We choose the central density to be 20 times bigger than the density at the boundary ρ_B to achieve a better resolution:

$$\rho_0 = 20\rho_B \tag{4.15}$$

$$20exp\left[\left(\frac{R}{R_0}\right)^2\right] = 1$$

$$\left(\frac{R}{R_0}\right)^2 = ln(20)$$

$$R_0 = \frac{R}{\sqrt{ln20}} = 0.58R \tag{4.16}$$

Hence the unperturbed initial density profile is:

$$\rho_i = \rho_0 exp\left[-\left(\frac{r}{0.58R}\right)^2\right] \tag{4.17}$$

where $\rho_0 = 5.0 \times 10^{18}g.cm^{-3}$ and $R = 7.5 \times 10^{16}cm \approx 0.02pc$. This density profile is also perturbed by the perturbation given in Eq. (4.6).

The initial cloud is in solid body rotation around the $\widehat{z}$ axis, with initial angular velocity $\Omega_0 = 5.4 \times 10^{-15}rad.s^{-1}$.

The magnetic field was chosen along the $\widehat{z}$-axis with strength in the range $B_0 = 0 - 200\mu G$.

For exponential density profile, simple analytical expressions for α (Eq. (4.1)) and

β (Eq. (4.2)). From dimensional analysis one could find:

$$\alpha \propto \frac{RT}{M} \tag{4.18}$$

$$\beta \propto \frac{\Omega^2}{\rho} \tag{4.19}$$

The radius R, the initial central density ρ_0, and the initial angular velocity Ω_0 are those of the model C3 from the paper by (A. P. Boss, 1987). This model was hydrodynamical with $\alpha = 0.39$ and $\beta = 0.000016$.

The equation of state used for these models is also a barotropic equation (Eq. (4.13)).

4.3   Method of calculations

One challenging aspect of a full MHD code is to preserve the divergence free condition of the magnetic field ($\boldsymbol{\nabla}.\boldsymbol{B} = 0$). It is important that this condition to be satisfied during the time step. Otherwise, a non-zero divergence can grow exponentially during the computation causing the Lorentz force to be non-orthogonal to the magnetic field (Brackbill & Barnes, 1980).

Trying to perform the numerical simulation and giving the fact that a construction of a numerical code is beyond the time limit of a master thesis, it was fortunate to get access to the so called "Enzo 2.4" code (Bryan et al., 2014). We used this **three-dimensional** code to solve the set of ideal MHD. It has a remarkable feature of adaptive mesh refinement (AMR) capability. This allows the code to "reach extremely large spatial and temporal dynamical ranges with limited compu-

tational resources, opening doors to applications otherwise closed by finite memory and computational time" (Bryan et al., 2014).

Two MHD methods are implemented in the `Enzo` code: the Dedner-based divergence cleaning (Dedner et al., 2002) and the Godunov MHD with Constrained Transport (CT) (C. R. Evans & Hawley, 1988).

We will work on the Dedner method. It ensures that $\boldsymbol{\nabla}.\boldsymbol{B} = 0$ for all time, provided it is so initially. This is accomplished by having $\boldsymbol{B}_0 = (B_{0x}, 0, 0)$ or , $\boldsymbol{B}_0 = (0, 0, B_{0z})$. The Enzo code solves the Poisson's equation for self-gravity using a fast Fourier technique (Hockney & Eastwood, 1988). It is done on the root grid on each timestep. The advantage of using this method is that it is fast, accurate, and naturally allows periodic boundary conditions for the gravity. The maximum number of Green's functions used to calculate the gravitational potential is 10, with 10 iterations performed on the gravitational potential at each step. This is to avoid over densities on the grid boundaries.

In the present calculations, the Enzo code is initialized on a 3D Cartesian grid with 64 grid points in each direction. So the initial resolution is 64^3. But we also permit a maximum of six levels of refinement with a refinement factor equals to 2. This means that the maximum effective resolution is $2^6 = 64$ times greater than the initial resolution. Hence, we get a maximum resolution of $(2^6 \times 64)^3 = 4096^3$. Finally, the time step used is 0.3 of the limiting Courant time step. This courant condition is used to ensure numerical stability in the time-explicit code. This timestep is embedded in Enzo, and it was not modified by hand.

Appendix B presents directions to getting, installing and running Enzo.

The visualization of the results were made using the yt-project (Turk et al., 2011).

Chapter 5

Results

We have performed three-dimensional MHD simulations using various initial conditions presented in the previous section. Since ideal MHD was adopted, the magnetic flux of the cloud remains constant throughout the collapse. This applies to the range of densities and magnetic field strengths adopted for the cloud models. In this chapter, we discuss the various results in terms of the effect of the magnetic field on the collapse of uniform density and centrally condensed clouds. After that, we investigate the degree to which the code conserved the mass, the angular momentum and the magnetic flux.

5.1   Uniform density

To investigate the effect of the magnetic field on the initially uniform cloud, calculations are performed with a gradually increasing magnetic field up to $400\mu G$. Table 5.1 summarizes the results at the critical density $\rho_c = 10^{-14} g.cm^{-3}$.

Model	$B_x\,(\mu G)$	$B_z\,(\mu G)$	t_c/t_{ff}	Result
hydro	0	0	1.230	thin bar with two cores
mag-z-20	0	20	1.2827	thin bar with two cores
mag-z-60	0	60	1.3403	two fragments with spiral arms
mag-z-80	0	80	1.3973	two fragments with spiral arms
mag-z-100	0	100	1.4054	two fragments with spiral arms
mag-z-300	0	300	1.4502	single with little spiral arms
mag-x-300	300	0	1.4986	single with significant spiral arms
mag-z-400	0	400	1.5229	single with spiral arms

Table 5.1: Initial magnetic field strengths (in Microgauss), the time t_c (in free fall time units) is the time when the density is $\rho_c = 10^{-14}g.cm^{-3}$ and the results at t_c for the collapse of uniform density MHD models with initial 10% density perturbations

In the table, the hydrodynamical model, neglecting the magnetic field, is named hydro. The magnetohydrodynamical models are named mag-(direction of magnetic field)-(strength of magnetic field). This follows the notation in BK13 and facilitates the comparison.

Table 5.1 shows that the main effect of increasing magnetic field is to delay the collapse of the initially slightly perturbed magnetized cloud. This is expected due to the fact that a magnetic field is a supporting agent against gravitational collapse. This result represents a nice test of the numerical simulation. The value of magnetic field is not strong enough to inhibit the collapse of the cloud, however it acts to delay the collapse.

It is interesting to find that for an initial magnetic field smaller than $200\mu G$,

the cloud undergoes fragmentation leading to a binary star formation). Whereas, for initial magnetic field strength larger than $200\mu G$, the cloud eventually collapsed to form a single protostar instead of a binary system. So the value of magnetic field determined whether or not the cloud form a single or binary system.

Another difference is that the collapse of the model mag-x-300 is slower than that of the model mag-z-300. This shows that the orientation of initial magnetic field also affects the evolution of the cloud, indicating that the star formation problem is indeed a three-dimensional problem. This is the way to describe the effect of the magnetic field in the collapsing cloud.

Although collapse is found in both models, there is an obvious difference between the outcomes. In mag-x-300, the collapse does not maintain a spherical symmetry like in the mag-z-300 case. Instead, it is somewhat elongated in the x-y plane (see Figure (5.1)). In fact, the density perturbation initially in the x-y plane will grow preferentially along the $\hat{x}$ axis, especially that the magnetic field is also along the $\hat{x}$ axis and particles will move more freely in the direction of the magnetic field lines. This results in a significant difference between the two model descriptions.

The outcomes of the hydro model and mag-z-20 model are the same, so that a $20\mu G$ initial magnetic field had a very small implication on the evolution of the cloud. Both models fragmented into two almost radial cores and then formed a bar-like configuration.

When the magnetic field is increased to $60\mu G$, $80\mu G$ and $100\mu G$, the spiral arms of the fragments accentuated. This is obviously due to the increase in magnetic field and not to the rotation of the cloud. This could be explained with magnetic

braking. When a high density region is connected to a low density region by magnetic field lines and is rotating faster than the background, magnetic field lines become twisted. The torque generated by this twist slows down the rotation of the high density material and transfers it to the low density medium around it. This would lead to the spiral arms we have noticed from our results.

Beyond the critical density, the fragments of all the models merged together and formed a final single protostar with spiral arms. For models with initial magnetic field $B_0 \geq 300\mu G$ the spiral arms have different shapes than the models with $B_0 \leq 300\mu G$. Figure 5.2 the outcome at the final time of all magnetized models. We clearly see the spiral arms in (a), (b), (c) and (d) have circular shapes, and (e) and (f) have more elongated shape. A $300\mu G$ magnetic field and above leads to a single protostar. We also tried $600\mu G$, but the simulation was heavy and slow, we reached $t = 2t_{ff}$ and the density had only increased by one order of magnitude. This suggests that the cloud was more magnetically supported.
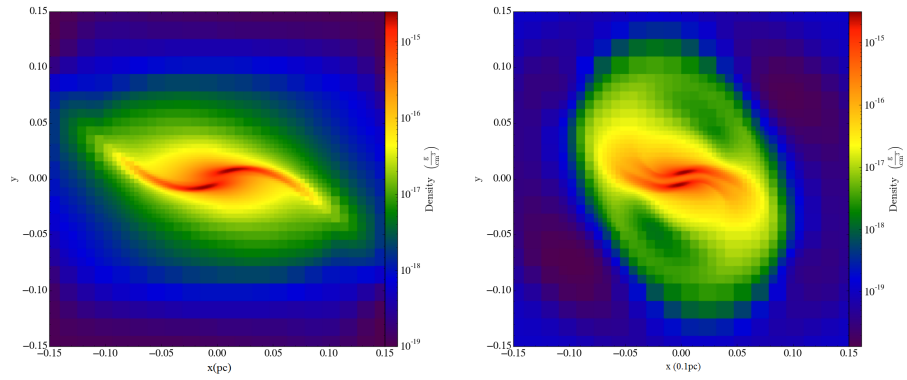
(a) mag-x-300 at $t = 1.4986t_{ff}$ (b) mag-z-300 at $t = 1.4127t_{ff}$

Figure 5.1: Collapse of a magnetized molecular cloud with two different orientation of the magnetic field along the x-axis (left panel) or along the z-axis (right panel). Symmetry of the outcome is obvious. (See text for details)

(a) mag-z-20 at $t = 1.4854 t_{ff}$ (b) mag-z-60 at $t = 1.5626 t_{ff}$

(c) mag-z-80 at $t = 1.6258 t_{ff}$ (d) mag-z-100at $t = 1.5868 t_{ff}$

(e) mag-z-300 at $t = 1.5537 t_{ff}$ (f) mag-z-400 at $t = 1.5910 t_{ff}$
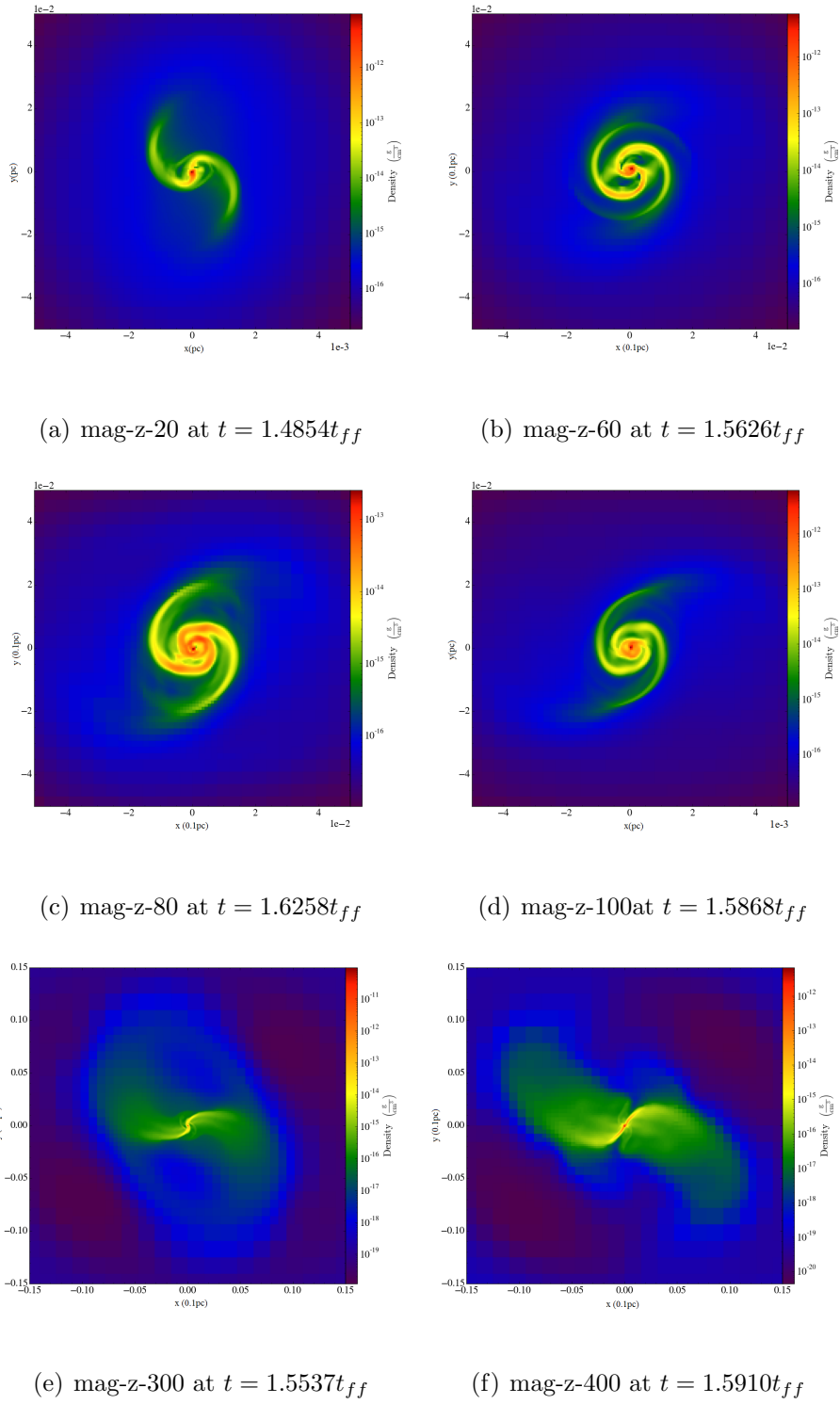
Figure 5.2: Outcome of the initial collapse phase of a magnetized uniform stellar cloud with variable magnetic field. Notice that (a) to (d) show circular shape, while (e) and (f) show elongated shapes.

Comparing our calculations with those obtained by BK13; we find the following:

Our simulations based on an isothermal equation of state (EOS, hereafter) as shown in Fig 5.2a and 5.2c are similar to the finding by BK13 on the basis of a barotropic EOS.

Using an isothermal EOS may be questioned due to radiative heating beyond the critical density. The fact that we get similar results with the isothermal EOS indicates that our results are reasonable up to the densities we have reached. However, further calculations will require a kind of radiative transport to be included or a suitable energy equation.

This discussion shows at least that our simulation was reasonably tested not only compared with other results, but also by using 3D Cartesian grid with 20 grid points in each direction, 32 and 64. The runs of these different grids converged into the same results.

5.2 Centrally condensed clouds

5.2.1 Flattened sphere density profile

In the following, we present the results of the initially flattened sphere (see Eq. (4.12)). Four models we investigated, and for each model several values of the magnetic field were introduced. Table (5.2) gives a summary of the results of each model. In this table, ρ_{max} is the maximum density at the final time t_f measured in units of t_{hydro} not in units of free fall time t_{ff}, where t_{hydro} is the final time for the

model with no magnetic field. This allows for an easier comparison, and conclusion concerning the question whether the magnetic field is able to delay the collapse process. The models with the lower initial central density are labeled "L", and higher initial central density are labeled "H". The models with the higher angular velocity are labeled "F" and the lower angular velocity are labeled "S". Then the magnetic field strength is mentioned in the name of the model. For the maximum density column, the number inside the parentheses is the power of ten, i.e. $10(-13)$ is 10^{-13}

For instance LS10 is the model with the lower density, slower rotation and magnetic field strength $10\mu G$.

For the LF models, the introduction of the magnetic field inhibited the fragmentation of the cloud, without delaying the collapse. The hydro model fragmented into a binary system, while including magnetic field the cloud collapsed into a single protostar.

All the LS models collapsed into a single protostar without spiral arms. And the delay in the collapse was larger than in the case of fast rotation.

All the H models, for both velocities, collapsed into a bar-like shape. For the hydro model, the bar has two cores. Regardless of the angular velocity of the cloud, the magnetic field (up to $B_0 = 100\mu G$) merely had no effect on the collapse. So we increased the magnetic field strength to $B_0 = 400\mu G$, which is still an observationally acceptable value for B. In this case, for both values of the rotation, the bar has a single core instead of two.

Figures 5.3, 5.4 and 5.5 illustrate these results also given in the table 5.2. To have an

$\rho_0(g.cm^{-3})$	$\Omega_0(rad.s^{-1})$	$B_0(\mu G)$	Model	$\rho_{max}(g.cm^{-3})$	t_f (t_{hydro})	Results
1.8×10^{-18}	2.9×10^{-13}	0	LF0	$10(-13)$	1.0000	Binary with spiral arms
		10	LF10	$10(-13)$	1.0188	Single with spiral arms
		100	LF100	$10(-13)$	1.0188	Single with spiral arms
	2.9×10^{-15}	0	LS0	$10(-12)$	1.0000	Single without spiral arms
		10	LS10	$10(-12)$	1.0047	Single without spiral arms
		100	LS100	$10(-12)$	1.0840	Single with supported surrounding
3.1×10^{-17}	2.9×10^{-13}	0	HF0	$10(-11)$	1.0000	Bar with two cores
		10	HF10	$10(-11)$	1.0019	Bar with two cores
		100	HF100	$10(-11)$	1.0257	Bar with two cores
		400	HF400	$10(-11)$	1.1502	Bar with one core
	2.9×10^{-15}	0	HS0	$10(-13)$	1.0000	Bar with two cores
		10	HS10	$10(-13)$	1.0000	Bar with two cores
		100	HS100	$10(-12)$	1.0090	Bar with two cores
		400	HS400	$10(-12)$	1.0322	Bar with one core

Table 5.2: Summary of the results of the collapse of the various flattened sphere models with 10% initial density perturbation

idea about the timescales of the problem, we first calculated the free fall timescale (Eq.(2.18)), only for the sake of comparison. We emphasize that this timescale is not realistic, because it is linked to uniform spherical density supported only by its thermal pressure. Also, from the simulations, we have the collapse timescale of the hydrodynamic models, t_{hydro}, that depends on both the initial central density and the initial angular velocity. These timescales are given in table (5.3)

$\rho_0(g.cm^{-3})$	$t_{ff}(yrs)$	$\Omega_0(rad.s^{-1})$	$t_{hydro}(yrs)$
1.8×10^{-18}	4.9618×10^4	2.9×10^{-13}	7.6142×10^4
		2.9×10^{-15}	6.4195×10^4
3.1×10^{-17}	1.1956×10^4	2.9×10^{-13}	1.2994×10^4
		2.9×10^{-15}	1.2063×10^4

Table 5.3: The free fall timescale and the collapse timescale of the hydrodynamic model

We note form the table that the faster the cloud's rotation is, the longer the collapse timescale is. This is understandable because the rotation is a supporting agent against gravity, like the magnetic field. Also, due to the extra support from rotation, t_{hydro} is bigger than t_{ff}. From table (5.2), the collapse time increases with increasing the magnetic field, due to the extra support added because of the magnetic pressure.

In summary, we have seen from the numerical models presented in this section that,in a flattened sphere, the main effect of the magnetic field is to inhibit

the formation of a binary system, along with delaying the collapse.

(a) $B = 0$ (b) $B = 10\mu G$

Figure 5.3: The collapse of the models with the lower density and the higher angular velocity with two different magnetic field strengths: A binary system (left panel) and a single protostar (right panel).

(a) $B = 0$ (b) $B = 100\mu G$

Figure 5.4: LThe collapse of the models with the lower density and the lower angular velocity with two different magnetic field strengths: A single protostar (left panel) and a single protostar with supported surrounding (right panel).

(a) $B = 0$ (b) $B = 400\mu G$

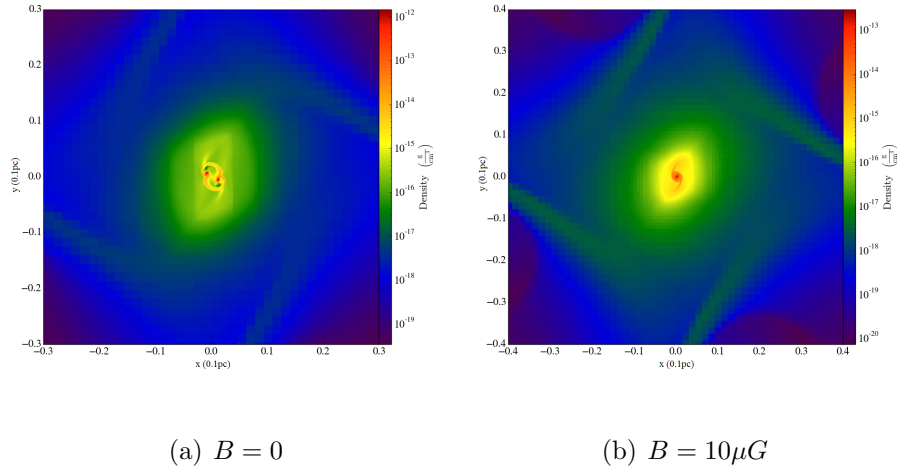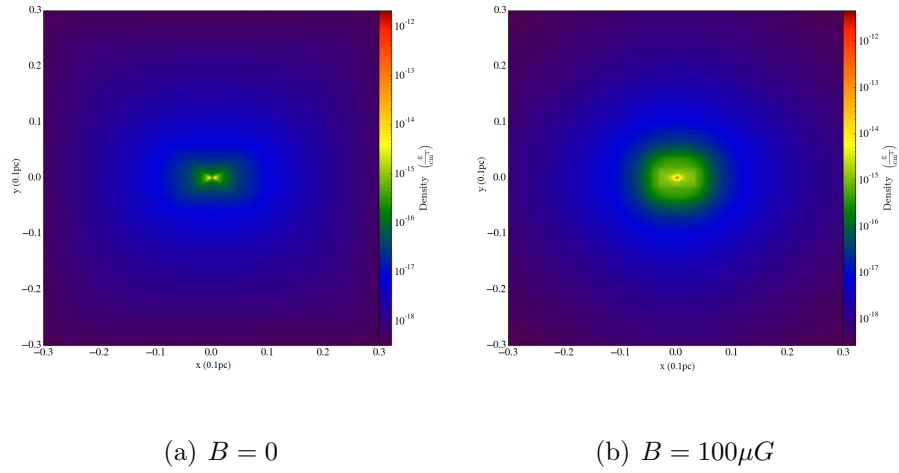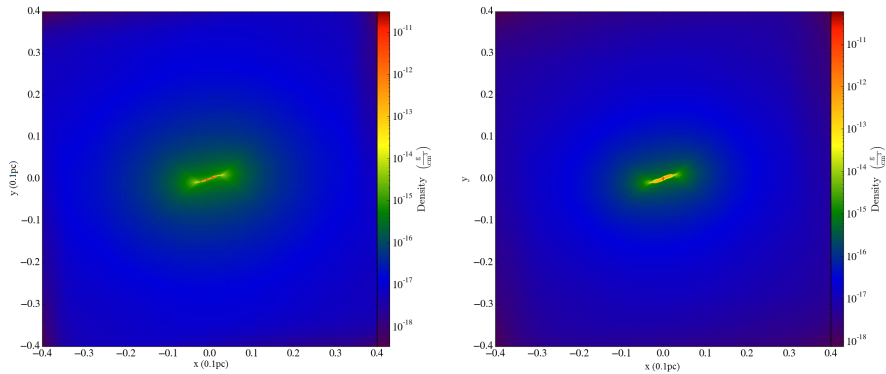Figure 5.5: The collapse of the models with the higher density and the higher angular velocity with two different magnetic field strengths: A bar with two cores (a) and a bar with one core (b)

5.2.2   Exponential density profile

This section presents the results of the collapse of the models with initial exponential density profile (see Eq. (4.17)). They are summarized in the table (5.4). The models are labeled with E followed by the magnetic field strength.

The main of effect of the magnetic field on a slowly rotating, initially exponentially decreasing density is to delay the collapse. However, the magnetic field did not influence the shape of the collapse. All the magnetized clouds collapsed into a point-like single protostar (see Figure (5.6)). This is the same outcome as the non-magnetized model. This indicates the important role of the initial density distribution of the effect of the magnetic field.

As the table shows, the time it took the cloud to collapse by 5 to 6 orders of magnitude increases by increasing the initial magnetic field strength.

The table also shows that with an initial magnetic field of strength $B_0 = 100\mu G$

54

$\rho_0 (g.cm^{-3})$	$\Omega_0 (rad.s^{-1})$	$B_0 (\mu G)$	Model	$\rho_{max}(g.cm^{-3})$	$t_f (t_{hydro})$	Results
		0	E0	10(−12)	1.0000	Point-like single protostar
		10	E10	10(−12)	1.1416	Point-like single protostar
		20	E20	10(−11)	1.2080	Point-like single protostar
5.0×10^{-18}	5.4×10^{-15}	40	E40	10(−11)	1.2097	Point-like single protostar
		60	E60	10(−12)	1.5291	Point-like single protostar
		80	E80	10(−12)	1.5316	Point-like single protostar
		100	E100	10(−17)	2.8033	Oscillation and no collapse
		200	E200	10(−17)	3.1855	Oscillation and no collapse

Table 5.4: Summary of the results of the collapse of the exponential initial density models with 10% initial density perturbation for different magnetic field strengths
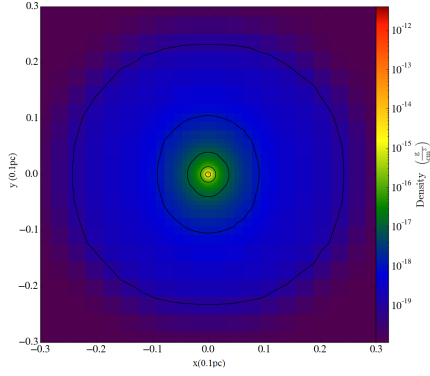
Figure 5.6: The point like final protostar for all collapsing models with initial exponential density

and higher, the cloud did not collapse. On the contrary, the cloud's maximum density oscillated between $10^{-17} g.cm^{-3}$ and $10^{-18} g.cm^{-3}$. Hence, for $B_0 \geq 100 \mu G$, the magnetic field supports the cloud against gravitational collapse. We note that for an non uniform density, it is harder to calculate a critical mass-to-flux ratio as it was the case for the uniform density (see Eq.(2.13)).

As for the timescales: $t_{ff} = 2.9771 \times 10^4 yrs$ and $t_{hydro} = 6.0882 \times 10^4 yrs$, then the collapse timescale of the magnetized clouds increases with increasing the magnetic field strength. Then for $B_0 \geq 100 \mu G$, the clouds remain stable even after $t_f = 3.9661 \times 10^5 yrs$.

To summarize, for an initially exponentially decreasing density, there exist a value for the magnetic field strength above which the cloud is stable. For our initial central density $\rho_0 = 5 \times 10^{-18} g.cm^{-3}$, the threshold of stability is $B_{stable} \geq 100 \mu G$. But the magnetic field did not alter the shape of the collapse, since all models collapsed into a point-like single protostar.

5.3 Conservation results

5.3.1 Mass and angular momentum conservation

After having ran all the simulations using the Enzo code, and presented the respective results in the sections above, we will test the runs for the conservation of mass, angular momentum and magnetic flux.

By design, Enzo is able to conserve mass and linear momentum(Bryan et al., 2014), since it is a Cartesian coordinate code. So we will check to which degree was the mass conserved in each of our runs. Furthermore, unlike other codes written in spherical or cylindrical coordinates, Enzo does not necessarily conserve angular momentum. Hence we also test here Enzo's ability to conserve angular momentum.

Table (5.5), (5.6) and (5.7) present for each model the mean change in mass and angular momentum in units of initial mass and initial angular momentum, respectively.

Model	$B_x\,(\mu G)$	$B_z\,(\mu G)$	$\Delta M(M_0)$	$\Delta J(J_0)$
hydro	0	0	-0.0039	-0.0084
mag-z-20	0	20	-0.0024	-0.0049
mag-z-60	0	60	-0.0121	-0.0026
mag-z-80	0	80	-0.0026	-0.0019
mag-z-100	0	100	-0.0042	-0.0028
mag-z-300	0	300	-0.0089	-0.0664
mag-x-300	300	0	-0.0038	-0.2838
mag-z-400	0	400	-0.0024	-0.1607

Table 5.5: The change in mass and angular momentum for the uniform sphere models

For the initial uniform sphere, the mass was conserved to the 0.5% level. For low magnetic field ($B_0 \leq 100\mu G$), the angular momentum was practically conserved to the 0.4% level. But for models mag-x-300 and mag-z-400, the change in angular momentum becomes 28% and 16%, respectively. This shows that the angular momentum was lost for high magnetic field. Even though, in reality angular momentum should be lost to solve the angular momentum problem, it should not do so numerically.

Closer investigations of mag-x-300 and mag-z-400 showed that the loss was at the very end after a very dense central core has formed. This suggests that the resolution might be the reason for this unacceptable loss of angular momentum. If this is the case, increasing the initial resolution of the simulation could minimize these

losses. In order to do so, the size of the initial grid was increased from 32^3 to 64^3, the refinement factor was also increased from 2 to 12 and the maximum levels of refinement from 6 to 16. This leads to an increase in resolution from $32^3 \times 2^6$ to $64^3 \times 12^{16}$. For this resolution, the loss in angular momentum becomes 0.021 and 0.041 for mag-x-300 and mag-z-400. Hence, although the resolution was enhanced significantly a loss in angular momentum was still present, but acceptable.

In BK13, the model mag-z-400-10 in table 3 is similar to the mag-z-400 in our simulations. The change in angular momentum obtained by BK13 was $\Delta J_{tot} = +9.7\%$. So the angular momentum wasn't lost but instead was increased by 9.7%. This might be due to the MHD solver or the version of Enzo used. In table 2, mag-z-300 and mag-x-300 are also similar to our models but with a larger initial perturbation (amplitude 50% instead of 10%). The model mag-z-300 in BK13 had $\Delta J_{tot} = -5.0\%$, close to the change obtained in this work for mag-z-300. We note that the final time in BK13 for this model is close to the final time in this work. On the contrary, the model mag-x-300 in BK13 lost 0.9% of the angular momentum only. This discrepancy could be due to the time of the simulation which was equal to $5.8t_{ff}$ in BK13 instead of $1.5t_{ff}$ in our work.

Why is the angular momentum lost during an MHD simulation?

Allen, Li, and Shu (2003) showed that angular momentum can be removed in a low-speed outflow driven by magnetic braking during the collapse, provided that the cloud is magnetized and the ideal MHD approximation holds. Also Hennebelle and Ciardi (2009) explained that due to magnetic braking, the magnetic field twist transports angular momentum outward and effectively outside of the computational

volume by virtue of the field handling on the boundaries of the cube.

Model	$\Delta M(M_0)$	$\Delta J(J_0)$
LF0	-0.0078	-0.0230
LF10	-0.0066	-0.0220
LF100	-0.0331	-0.0185
LS0	-0.0200	-0.0459
LS10	-0.0052	-0.0544
LS100	-0.0053	-0.0855
HF0	-0.0056	-0.0266
HF10	-0.0056	-0.0267
HF100	-0.0054	-0.0265
HF400	-0.0049	-0.0471
HS0	-0.0044	-0.0164
HS10	-0.0045	-0.0164
HS100	-0.0049	-0.0164
HS400	-0.0045	-0.0322

Table 5.6: The change in mass and angular momentum for the flattened sphere models

As for the flattened sphere, both the mass and the angular momentum were conserved, to the 0.8% and to the 3% level, respectively.

Model	$\Delta M(M_0)$	$\Delta J(J_0)$
E0	-0.0646	-0.0849
E10	-0.0715	-0.0234
E20	-0.0708	-0.0866
E40	-0.0755	-0.0883
E60	-0.0892	-0.1126
E80	-0.0924	-0.1146
E100	-0.1077	-0.1946
E200	-0.0831	-0.1538

Table 5.7: The change in mass and angular momentum for the exponential density models

In the case of the exponentially decreasing density, the change in mass was 8% and the change in angular momentum is 10%. The loss of angular momentum increased with increasing magnetic field strength. This again shows that as the loss of the angular momentum is related to the magnetic field and rotation. As explained earlier, it is actually due to the magnetic braking process where the angular momentum is pushed away from the protostar.

5.3.2 Magnetic flux conservation

Magnetic field is a divergence free field ($\nabla.B = 0$), so the magnetic flux should be conserved in the ideal MHD picture. So, in this section, we test for the magnetic flux conservation. In order to do that, we will investigate the parameter

$\frac{(\nabla.B).dx}{B}$ instead of $\nabla.B$. The advantage of doing so is that this parameter is dimensionless. Knowing that "zero" cannot be reached numerically, using a dimensionless parameter would give insight about the quantity regardless of the problem studied. So this parameter should be a lot smaller than 1.

In our simulations, we use the Dedner et al. (2002) divergence cleaning method (Wang, Abel, & Zhang, 2008). This method does not conserve the magnetic field to a very high level. Even if $\nabla.B = 0$ initially, $\nabla.B$ does not stay zero throughout the simulation. It actually peaks when a region becomes very dense, as also observed in BK13. But Wang and Abel (2009) has shown that the non-zero field divergence that arises during a typical calculation is not large enough to be dynamically important. And to make sure this is true, we monitor the $\frac{(\nabla.B).dx}{B}$ parameter. The constrained transport MHD (Collins, Xu, Norman, Li, & Li, 2010) method could be more accurate than the cleaning method.

We tested all the runs for the magnetic flux conservation, and in the worst case scenario the parameter $\frac{(\nabla.B).dx}{B}$ is of the order of 10^{-3}. This means that the divergence of the magnetic field is zero to the 0.1% level. In average, this parameter is in the range $10^{-3} - 10^{-6}$. These values are typical for a cleaning method. Thus, this shows that the magnetic field was conserved reasonably well.

Chapter 6

Conclusion and Future Work

The work in this thesis can be divided into two categories:

1. Idealized settings: A rigidly rotating uniform magnetized stellar cloud with isothermal equation of state.

2. More realistic initial conditions: Rigidly rotating centrally condensed magnetized stellar clouds with polytropic equation of state.

The standard theory of gravitational collapse of a magnetized cloud consists of a subcritical cloud unable to collapse because of the magnetic field support against gravity. But, due to ambipolar diffusion, described in section 2.3.1, this cloud could eventually collapse under its own gravity.

However, the theory of ambipolar diffusion does not give a unified explanation of the collapse for both high and low mass clouds. Furthermore, the most recent observations of interstellar magnetic fields didn't find any proof of the ambipolar diffusion driven cloud collapse. And molecular clouds were found to be supercritical

or slightly critical. Hence, the so called "standard theory" of star formation was no longer thought to be relevant in stellar formation.

In sect (3.3), the diffusion terms of the induction equation were estimated for the densities and magnetic field strengths considered in the present work. These terms were found small enough to be neglected: Ohmic resistivity term was of the order of $10^{-47}G/s$, and the ambipolar diffusion term was of the order of $10^{-21}G/s$. Hence, we found arguments in favor of using the ideal MHD approximation. We emphasize that this conclusion does not necessarily rule out ambipolar diffusion from the theory of star formation. The ambipolar diffusion term for low densities and high magnetic field can become of the order of $10^{-11}G/s$. And in this range the ideal MHD will no longer be a valid approximation.

In the first part of the thesis, we reproduced the MHD model according to A. Boss and Keiser (2013) using an isothermal equation of state. In the second part, we considered a more realistic model with a more realistic equation of state (EOS). This was a centrally condensed clouds, with barotropic EOS. This latter mimic the non-isothermal effects arising when the density is higher than $10^{-14}gcm^{-3}$. This EOS, although not totally accurate, is more realistic than a pure isothermal equation of state. An energy equation should be used to fully understand the radiative transfer processes, which is subject to future considerations.

We first summarize the results of the uniform density cloud as follows: Using the isothermal equation of state is only accurate for densities below the critical

density ρ_c, so the results of the magnetized models are first compared for $\rho_{max} = \rho_c$ (see table 5.1), then compared at the final time where $\rho_{max} > \rho_c$.

1. At $\rho_{max} = \rho_c$, models with magnetic field strength below a critical value $B_c = 200\mu G$ formed binary systems. In contrast, for $B > B_c$, the models had collapsed into a single system.

2. At the final time where $\rho_{max} > \rho_c$, all the models collapsed into a single protostar with spiral arms. The models with $B < B_c$, the spirals are circular, while the models with $B < B_c$, the spirals are more elongated (see figure5.2).

3. The main effect of the magnetic field was found to delay the collapse of the clouds. This is expected because the magnetic field supports the cloud against collapse by increasing the gas pressure.

4. If the magnetic field is taken perpendicular to the axis of rotation, the collapse was delayed longer than when the field was parallel. The cloud was no more spherical like in the x-y plane, it became elongated. The reason is that the particles are able to move easily along the direction of the field.

The results of the more realistic centrally condensed clouds are summarized as follows:

1. For the flattened sphere density profile (see Eq. 4.12):

   (a) The main effect of the magnetic field in all models was to inhibit the formation of binary systems. The models with zero magnetic field formed

with two cores, while for stronger magnetic field they formed a bar with one core.

(b) We also noticed a slight delay in the collapse with increasing magnetic field. This effect was not as important for this initial condition than it was for uniform initial density.

2. For the exponentially decreasing density profile (see eq. (4.17)):

(a) For these models, we found a critical magnetic field $B_c = 100\mu G$. For $B < B_c$, the collapse was delayed with increasing magnetic field. Whereas, for $B \geq B_c$, the cloud did not collapse, and the magnetic field was able to stabilize the clouds.

(b) The magnetic field did not affect the shape of the collapse. All the models collapsed into a point-like single protostar.

Finally, we conclude the effect of magnetic field on the collapse of a molecular cloud in **the ideal MHD approximation** as follows:

1. If the unmagnetized cloud collapses into a single protostar and the magnetic field is not strong enough to inhibit its collapse, the magnetic field delays it. While, if the magnetic field is strong enough, the cloud is stable against gravitational collapse.

2. If the unmagnetized cloud collapses into a binary system, the magnetic field leads to a final single protostar.

We emphasize that these results may not be the same if the non-ideal MHD is used. In the non-ideal MHD picture, fragmentation could be enhanced, because not all the cloud would have the same magnetic support. And regions of the cloud would be more prone to collapse, while other regions would stay magnetically supported.

We tested for the conservation of mass, angular momentum and magnetic flux.

1. Mass conservation: By design, Enzo conserves the mass, and we found that the mass was indeed conserved to the 0.8% level as an average for all the runs.

2. Angular momentum conservation: Enzo does not necessarily conserve angular momentum because it a Cartesian code. Angular momentum was conserved for some runs, and for other runs with higher magnetic field angular momentum was lost between 18 and 25%. An increase in the resolution minimized this loss to 2.1% and 4.1%.

3. Magnetic flux conservation: To solve the MHD set of equation a cleaning method was used, during which the magnetic flux was conserved to the 10^{-6} or the 10^{-3} level. Keeping the magnetic field divergence free would be more efficient if the method used is the Constrained Method which is very accurate (to the 10^{-15} level). But the problem with this method is that it crashes more often, while the cleaning method is more stable.

In a future perspective, it is important to add an energy equation to fully study the radiative transfer in magnetized clouds. Also, it is interesting to investi-

gate a differential rotation instead of a solid body rotation.

Also, an interesting application of the present approach is to investigate the formation of early stars in the universe. The dark age started 380000 yr after Big Bang and lasted 400 million years. The first stars were formed reionizing the medium. The nature of the first star is not well known, especially their mass range. An interesting review on this subject is given by Bromm (2013).

Appendix A

The induction equation

In order to derive the induction equation in the subsection 3.1.1, the Ampere's law was used (Eq. (3.8)) and the displacement current $\left(\dfrac{\partial D}{\partial t}\right)$ from Maxwell's equations is neglected. A. P. Boss (1997) showed that this term can be neglected for a long timescale process such as ambipolar diffusion, if the conductivity of the medium is very high. In this appendix, we evaluate the value of the electrical conductivity in typical molecular clouds.

The electrical conductivity is given by σ_e (Tanenbaum, 1967):

$$\sigma_e = \frac{n_e e^2}{m_e \nu} \tag{A.1}$$

where n_e is the number density of electrons, e is the electron charge, m_e is the

electron mass and ν is the electron-neutral collision frequency. ν given by:

$$\nu = 4.5 \times 10^{-9} n_n \left(\frac{T_e}{300} \right)^{1/2} \tag{A.2}$$

where n_n is the neutrals number density and T_e is the electron temperature roughly equal the gas temperature T.

Eq. (A.2) in Eq. (A.1) gives the conductivity as a function of temperature and ionization:

$$\sigma_e = 6 \times 10^{16} x_i \left(\frac{300}{T} \right)^{1/2} \tag{A.3}$$

where $x_i = n_e/n_n$ is the fractional ionization.

For typical values of x_i and T in molecular clouds, the electrical conductivity is very high close to $\sigma_e \approx 3 \times 10^{10}$.

For this large value of conductivity, the displacement current $\left(\frac{\partial D}{\partial t} \right)$ in Maxwell's equations can be neglected for long timescale phenomena such as ambipolar diffusion

(A. P. Boss, 1997).

Appendix B

Enzo code

In this thesis, we performed the numerical simulations to solve the set of ideal MHD using the publicly available Enzo code[1]. In this chapter, we present a quick guide to obtaining, building and running this code. After that, we test the code on exactly solvable problem.

B.1   Obtaining and building the code

First, necessary libraries have to be obtained in order to run the code:

1. HDF5: When compiling HDF5, do not enable parallel, as Enzo is not compatible with that, and it won't compile.

2. MPI: Although, Enzo compiles without MPI, having MPI for multi-processor parallel jobs allows computation that would otherwise take infinite computa-

---

[1]http://enzo-project.org

tion time to complete.

3. Mercurial: It will be needed for a straightforward download of Enzo. This is what the hg command stand for.

4. yt: It is a visualization and analysis tool that enables the easiest analysis of Enzo outputs.

Now, run the following command to make a copy of the existing Enzo source code :

~ $ hg clone https://bitbucket.org/enzo/enzo-stable

After having downloaded Enzo, you must initialize the Build System and this is by running the configuration tool.:

~/enzo-stable $ ./configure

Now in order to build the Makefile, go and choose the machine-specific configuration from the list Make.mach.*.

~/enzo-stable/src/enzo $ make machine-linux-gnu

~/enzo-stable/src/enzo $ make

The last command compiles the code and creates an executable file "enzo.exe" in the current directory.

It is now straightforward to build the two other tools for enzo: inits and ring. Inits creates the initial conditions for your simulation, and ring splits up the root grid which is necessary if you're using parallel IO.

~/enzo-stable/src/inits $ make

~/enzo-stable/src/ring $ make These two commands create inits.exe and ring.exe respectively in the inits and ring directories.

B.2   Running the code

In the run directory, there are several test problems each for a problem type, like: Kelvin-Helmholtz instability, the collapse of a rotating cylinder, spherical infall, pressureless collapse, gravity equilibrium test, shearing box simulation, as well as several radiation-hydrodynamics tests.

The Enzo test case of interest to this thesis work is the 3 dimensional Magneto-Hydro-Dynamical collapse.

Two C++ programs initialize our problem: CollapseMHD3DInitialize.C and Grid_CollapseMHD3DInitializeGrid.C. The problem type is 202.

Generally, the *Problem*Initialize.C program reads the problem-specific parameters from the *Problem*.enzo file. Then the Grid_*Problem*InitializeGrid.C initializes the grid by setting the parameters of every cell and adding any particles that are needed at the simulation start.

References

Adams, F. C., & Shu, F. H. (2007). Ambipolar diffusion in molecular cloud cores and the gravomagneto catastrophe. *The Astrophysical Journal*, *671*(1), 497.

Allen, A., Li, Z.-Y., & Shu, F. H. (2003). Collapse of magnetized singular isothermal toroids. ii. rotation and magnetic braking. *The Astrophysical Journal*, *599*(1), 363.

Basu, S. (1997). A semianalytic model for supercritical core collapse: Self-similar evolution and the approach to protostar formation. *The Astrophysical Journal*, *485*(1), 240.

Basu, S., & Mouschovias, T. C. (1994). Magnetic braking, ambipolar diffusion, and the formation of cloud cores and protostars. 1: Axisymmetric solutions. *The Astrophysical Journal*, *432*, 720–741.

Benson, P., & Myers, P. (1989). A survey for dense cores in dark clouds. *the Astrophysical Journal Supplement Series*, *71*, 89–108.

Boss, A., & Bodenheimer, P. (1979). Fragmentation in a rotating protostar-a comparison of two three-dimensional computer codes. *The Astrophysical Journal*, *234*, 289–295.

Boss, A., & Keiser, S. A. (2013). Collapse and fragmentation of magnetic molecular cloud cores with the enzo amr mhd code. i. uniform density spheres. *The Astrophysical Journal*, *764*(2), 136.

Boss, A. P. (1987). Protostellar formation in rotating interstellar clouds. VI-nonuniform initial conditions. *The Astrophysical Journal*, *319*, 149–161.

Boss, A. P. (1997). Collapse and fragmentation of molecular cloud cores. v. loss of magnetic field support. *The Astrophysical Journal*, *483*(1), 309.

Brackbill, J. U., & Barnes, D. C. (1980). The effect of nonzero divergence of B on the numerical solution of the magnetohydrodynamic equations. *Journal of Computational Physics*, *35*(3), 426–430.

Braiding, C. (2011). Star formation and the hall effect. *arXiv preprint arXiv:1110.2168*.

Brandenburg, A., & Zweibel, E. (1994). The formation of sharp structures by ambipolar diffusion. *The Astrophysical Journal*, *427*, L91–L94.

Brandenburg, A., & Zweibel, E. G. (1995). Effects of pressure and resistivity on the ambipolar diffusion singularity: too little, too late. *The Astrophysical Journal*, *448*, 734.

Bromm, V. (2013). Formation of the first stars. *Reports on Progress in Physics*, *76*(11), 112901.

Bryan, G. L., Norman, M. L., O'Shea, B. W., Abel, T., Wise, J. H., Turk, M. J., ... The Enzo Collaboration (2014, April). Enzo: An adaptive mesh refinement code for astrophysics. *The Astrophysical Journal*, *211*, 19. doi: 10.1088/0067-0049/211/2/19

Chandrasekhar, S., & Fermi, E. (1953). Problems of gravitational stability in the presence of a magnetic field. *Astrophysical Journal*, 116–141.

Choi, K. J., E., & Wiita, P. J. (2009). An explicit scheme for incorporating ambipolar diffusion in a magnetohydrodynamics code. *The Astrophysical Journal Supplement Series*, *181*(2), 413.

Collins, D. C., Xu, H., Norman, M. L., Li, H., & Li, S. (2010). Cosmological adaptive mesh refinement magnetohydrodynamics with enzo. *The Astrophysical Journal Supplement Series*, *186*(2), 308.

Crutcher, R. M. (1999). Magnetic fields in molecular clouds: observations confront theory. *The Astrophysical Journal*, *520*(2), 706.

Crutcher, R. M. (2012). Magnetic fields in molecular clouds. *Annual Review of Astronomy and Astrophysics*, *50*, 29–63.

Crutcher, R. M., Hakobian, N., & Troland, T. H. (2009). Testing magnetic star formation theory. *The Astrophysical Journal*, *692*(1), 844.

Dalgarno, A. (2006). The galactic cosmic ray ionization rate. *Proceedings of the National Academy of Sciences*, *103*(33), 12269–12273.

Dedner, A., Kemm, F., Kröner, D., Munz, C., Schnitzer, T., & Wesenberg, M. (2002). Hyperbolic divergence cleaning for the mhd equations. *Journal of Computational Physics*, *175*(2), 645–673.

Evans, C. R., & Hawley, J. F. (1988). Simulation of magnetohydrodynamic flows-a constrained transport method. *The Astrophysical Journal*, *332*, 659–677.

Evans, N. J. (1999). Physical conditions in regions of star formation. *Annual Review of Astronomy and Astrophysics*, *37*, 311–362.

Fiedler, R. A., & Mouschovias, T. C. (1992). Ambipolar diffusion and star formation: formation and contraction of axisymmetric cloud cores. i-formulation of the problem and method of solution. *The Astrophysical Journal*, *391*, 199.

Fiedler, R. A., & Mouschovias, T. C. (1993). Ambipolar diffusion and star formation: formation and contraction of axisymmetric cloud cores. ii. results. *The Astrophysical Journal*, *415*, 680.

Field, G. (1982). Conditions in collapsing clouds. In *Protozvezdy i planet. issled. obraz. zvezd i proiskhozhd. soln. sist.* (Vol. 1, pp. 274–294).

Froebrich, D. D. (2015, Spring). *Graduate course: Ph712-cosmology and interstellar medium.* University of Kent - the UK's European university.

Fuller, G., & Myers, P. (1992). Dense cores in dark clouds. vii-line width-size relations. *The Astrophysical Journal*, *384*, 523–527.

Greaves, J. S., & Holland, W. S. (1999). Ambipolar diffusion in magnetized cloud cores. *Monthly Notices of the Royal Astronomical Society*, *302*(3), L45–L48.

Hennebelle, P., & Ciardi, A. (2009). Disk formation during collapse of magnetized protostellar cores. *Astronomy & Astrophysics*, *506*(2), L29–L32.

Hockney, R. W., & Eastwood, J. W. (1988). *Computer simulation using particles.* CRC Press.

Inutsuka, S.-i. (2012). Present-day star formation: From molecular cloud cores to protostars and protoplanetary disks. *Progress of Theoretical and Experimental Physics*, *2012*(1), 01A307.

Jeans, J. (1902). The stability of a spherical nebula. *Royal Society of London Philosophical Transactions Series A*.

Joos, M., Hennebelle, P., & Ciardi, A. (2012). Protostellar disk formation and transport of angular momentum during magnetized core collapse. *Astronomy & Astrophysics*, *543*, A128.

Kim, J. (2011). A fast explicit scheme for solving mhd equations with ambipolar diffusion. In *Computational star formation* (Vol. 270, pp. 415–419).

Klessen, R. S., Heitsch, F., & Mac Low, M.-M. (2000). Gravitational collapse in turbulent molecular clouds. i. gasdynamical turbulence. *The Astrophysical Journal*, *535*(2), 887.

Krumholz, M. R. (2011). Star formation in molecular clouds. *arXiv preprint arXiv:1101.5172*.

Kudoh, T., Basu, S., Ogata, Y., & Yabe, T. (2007). Three-dimensional simulations of molecular cloud fragmentation regulated by magnetic fields and ambipolar diffusion. *Monthly Notices of the Royal Astronomical Society*, *380*(2), 499–505.

Larson, R. B. (1993). The evolution of molecular clouds. In T. L. Wilson & K. J. Johnston (Eds.), *The structure and content of molecular clouds 25 years of molecular radioastronomy.*

Lazarian, A. (2005). Astrophysical implications of turbulent reconnection: from cosmic rays to star formation. *arXiv preprint astro-ph/0505574.*

Li, Z.-Y., Krasnopolsky, R., & Shang, H. (2013). Does magnetic-field-rotation misalignment solve the magnetic braking catastrophe in protostellar disk formation? *The Astrophysical Journal, 774*(1), 82.

Li, Z. Y., & Shu, F. H. (1997). Self-similar collapse of an isopedic isothermal disk. *The Astrophysical Journal, 475*(1), 237.

Lizano, S., & Shu, F. H. (1989). Molecular cloud cores and bimodal star formation. *The Astrophysical Journal, 342*, 834–854.

Mac Low, M., & Klessen, R. S. (2004). Control of star formation by supersonic turbulence. *Reviews of modern physics, 76*(1), 125.

McKee, C. F., Zweibel, E. G., Goodman, A. A., & Heiles, C. (1993). Magnetic fields in star–forming regions–theory. In *Protostars and planets III* (Vol. 1, p. 327).

Mestel, L. (1999). *Stellar magnetism. clarendon.* Oxford.

Mestel, L., & Spitzer, L. (1956). Star formation in magnetic dust clouds. *Monthly Notices of the Royal Astronomical Society, 116*(5), 503–514.

Mouschovias, T. C. (1987). *Star formation in magnetic interstellar clouds: I. interplay between theory and observations.* Springer.

Mouschovias, T. C. (1991). Magnetic braking, ambipolar diffusion, cloud cores, and star formation-natural length scales and protostellar masses. *The Astrophysical Journal, 373*, 169–186.

Mouschovias, T. C., & Spitzer, L. J. (1976). Control of star formation by supersonic turbulence. *The Astrophysical Journal, 210*, 326.

Mouschovias, T. C., Tassis, K., & Kunz, M. W. (2006). Observational constraints on the ages of molecular clouds and the star formation timescale: Ambipolar-diffusion-controlled or turbulence-induced star formation? *The Astrophysical Journal, 646*(2), 1043.

Myers, P. C. (1985). Molecular cloud cores. In D. C. Black & M. S. Matthews (Eds.), *Protostars and planets ii* (p. 81-103).

Nakamura, F., & Li, Z. Y. (2005). Quiescent cores and the efficiency of turbulence-accelerated, magnetically regulated star formation. *The Astrophysical Journal, 631*(1), 411.

Nakano, T., & Tademaru, E. (1972). Decoupling of magnetic fields in dense clouds with angular momentum. *The Astrophysical Journal*, *173*, 87.

Norman, C., & Silk, J. (1980). Clumpy molecular clouds-a dynamic model self-consistently regulated by t tauri star formation. *the Astrophysical Journal*, *238*, 158–174.

Price, D. J., & Bate, M. R. (2007). The impact of magnetic fields on single and binary star formation. *Monthly Notices of the Royal Astronomical Society*, *377*(1), 77–90.

Shu, F. H., Adams, F. C., & Lizano, S. (1987). Star formation in molecular clouds - Observation and theory. *Ann. Rev. Astron. Astrophys.*, *25*, 23-81.

Spitzer, L., & Tomasko, M. G. (1968). Heating of hi regions by energetic particles. *The Astrophysical Journal*.

Tanenbaum, B. S. (1967). *Plasma physics.* McGraw-Hill.

Tassis, K., & Mouschovias, T. C. (2004). Ambipolar-diffusion timescale, star formation timescale, and the ages of molecular clouds: is there a discrepancy? *The Astrophysical Journal*, *616*(1), 283.

Troland, T. H., & Crutcher, R. M. (2008). Magnetic fields in dark cloud cores: Arecibo oh zeeman observations. *The Astrophysical Journal*, *680*(1), 457.

Turk, M. J., Smith, B. D., Oishi, J. S., Skory, S., Skillman, S. W., Abel, T., & Norman, M. L. (2011, January). yt: A Multi-code Analysis Toolkit for Astrophysical Simulation Data. *The Astrophysical Journal*, *192*, 9-+.

Vázquez-Semadeni, E., Gómez, G. C., Jappsen, A. K., Ballesteros-Paredes, J., González, R. F., & Klessen, R. S. (2007). Molecular cloud evolution. ii. from cloud formation to the early stages of star formation in decaying conditions. *The Astrophysical Journal*, *657*(2), 870.

Viti, E., S.and Bayet, Hartquist, T. W., Bell, T. A., Williams, D. A., & Banerji, M. (2013). Cosmic rays in the interstellar medium. In *Cosmic rays in star-forming environments* (pp. 7–20). Springer.

Wang, P., & Abel, T. (2009). Magnetohydrodynamic simulations of disk galaxy formation: the magnetization of the cold and warm medium. *The Astrophysical Journal*, *696*(1), 96.

Wang, P., Abel, T., & Zhang, W. (2008). Relativistic hydrodynamic flows using spatial and temporal adaptive structured mesh refinement. *The Astrophysical Journal Supplement Series*, *176*(2), 467.

Wardle, M. (2004). Star formation and the hall effect. *Astrophysics and Space Science*, *292*(1-4), 317–323.

Ward-Thompson, D., André, P., Crutcher, R., Johnstone, D., Onishi, T., & Wilson, C. (2007). An observational perspective of low-mass dense cores ii: Evolution toward the initial mass function. *Protostars and Planets V*, *1*, 33–46.

Webber, W. (1998). A new estimate of the local interstellar energy density and ionization rate of galactic cosmic cosmic rays. *The Astrophysical Journal*, *506*(1), 329.

Whitworth, A. P., & Ward-Thompson, D. (2001). An empirical model for protostellar collapse. *The Astrophysical Journal*, *547*(1), 317.

Zuckerman, B., & Palmer, P. (1974). Radio radiation from interstellar molecules. *Annual Review of Astronomy and Astrophysics*, *12*, 279–313.